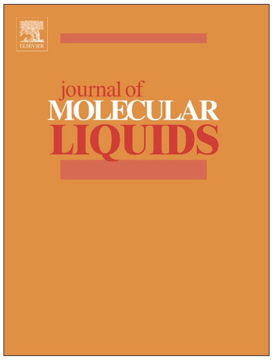

Optimizing density, dynamic viscosity, thermal conductivity and specific heat of a hybrid nanofluid obtained experimentally via ANFIS-based model and modern optimization

Zafar Said, L. Syam Sundar, Hegazy Rezk, Ahmed M. Nassef, Hafiz Muhammad Ali, Mohsen Sheikholeslami

PII:	S0167-7322(20)33923-4
DOI:	https://doi.org/10.1016/j.molliq.2020.114287
Reference:	MOLLIQ 114287
To appear in:	*Journal of Molecular Liquids*
Received date:	16 June 2020
Revised date:	6 September 2020
Accepted date:	8 September 2020

Please cite this article as: Z. Said, L.S. Sundar, H. Rezk, et al., Optimizing density, dynamic viscosity, thermal conductivity and specific heat of a hybrid nanofluid obtained experimentally via ANFIS-based model and modern optimization, *Journal of Molecular Liquids* (2018), https://doi.org/10.1016/j.molliq.2020.114287

Optimizing Density, Dynamic Viscosity, Thermal Conductivity and Specific Heat of a Hybrid Nanofluid obtained experimentally via ANFIS-based Model and Modern Optimization

Zafar Said[1, *], L. Syam Sundar[2], Hegazy Rezk[3, 4], Ahmed M. Nassef[3, 5], Hafiz Muhammad Ali[6], Mohsen Sheikholeslami[7]

[1]Department of Sustainable and Renewable Energy Engineering, University of Sharjah, P.O. Box 27272, Sharjah, United Arab Emirates

[2]Centre for Mechanical Technology and Automation (TEMA–UA), Department of Mechanical Engineering, University of Aveiro, 3810-131 Aveiro, Portugal

[3]College of Engineering at Wadi Addawaser, Prince Sattam Bin Abdulaziz University, Kingdom of Saudi Arabia

[4]Electrical Engineering Department, Faculty of Engineering, Minia University, Egypt

[5]Computers and Automatic Control Engineering Department, Faculty of Engineering, Tanta University, Egypt

[6]Mechanical Engineering Department, King Fahd University of Petroleum and Minerals, Dhahran 31261, Saudi Arabia

[7]Department of Mechanical Engineering, Babol Noshirvani University of Technology, Babol, Iran

***Corresponding authors: zsaid@sharjah.ac.ae; zaffar.ks@gmail.com**

Abstract

In this study, rGO/Co_3O_4 nanocomposite was synthesized, characterized, and then the thermophysical properties were obtained experimentally, after which the experimental data at varying values of temperature and particle loadings was used for optimization purposes. The study was concerned with different values of the controlling parameters. The *in-situ*/chemical reduction technique was used to synthesize the rGO/Co_3O_4 nanocomposite and then characterized with x-ray diffraction, transmission electron microscope, and magnetometry. The system was studied at temperature values ranging at 20, 30, 40, 50, and 60 ℃ and with particle loadings of 0.05%, 0.1%, and 0.2% wt.%. The authors in this article have introduced a novel population-based algorithm that is known as Marine Predators Algorithm to obtain the optimal values of the controlling parameters (i.e., temperature and nanofluid mixture percentage) that minimize two controlled variables (i.e., density and viscosity) as well as maximize the other two controlled variables (thermal conductivity and specific heat). The rGO/Co_3O_4 nanocomposite nanofluid thermal conductivity and viscosity were investigated experimentally, and a maximum increment of 19.14% and 70.83% with 0.2% particle loadings at 60^{o}C was obtained. At 0.05%, 0.1%, and 0.2% particle loading wt.%, the density increased by 0.115%, 0.23%, and 0.451% at a temperature of 20℃; simultaneously, density increased by 0.117%%, 0.235%, and 0.469% at 60℃, respectively as compared to water. At 0.2 wt.%, the maximum decreased specific heat was 0.192% and 0.194% at 20^{o}C and 60^{o}C. When compared with water, no effect was observed with an increase in temperature/: a similar trend as that of the water was followed. The optimal values were found to be at a temperature of 60℃ and for 0.05% particle loading of the prepared nanofluid. However, among the conducted experiments, the optimizer pointed out that the optimal experiment was the one conducted at a temperature of 60℃ and a nanofluid percentage at 0.05. In conclusion, the proposed methodology of modelling with an artificial intelligence tool such as an adaptive network-based fuzzy inference system technique and then determining the optimal parameters with the marine predators algorithm accomplished the goal of the study with major success.

Keywords: nanofluid, hybrid, graphene, parameter estimation, ANFIS, optimization

1. Introduction

Thermal plants and petrochemical applications have been using traditional heat exchangers by operating single-phase fluids such as water, ethylene glycol, propylene glycol, and engine oil as heat transfer fluids [1]. Low thermal conductivity single-phase fluids used in the conventional heat exchangers generate low efficiency. The efficiency can be enhanced by utilizing fluids with high thermal conductivity, such as nanofluids [2, 3]. Nanofluids are defined as the suspension of nanometer-sized particles in the base fluid and are reported to have higher thermal conductivity as compared to single-phase fluids [4, 5]. The thermal conductivity of the fluid has a direct impact on the heat transfer coefficient [6], so when the thermal conductivity increases, there is an enhancement in the heat transfer coefficient [7-9]. The thermal conductivity of nanofluids depends on the thermal conductivity of particle [10] and base fluid [11], with a fixed amount of heat supply, but the thermal conductivity of the particle has more impact on the enhancement of thermal conductivity [12, 13]. Several nanoparticles such as Al_2O_3, Cu, CuO, carbon-based, Co_3O_4, Fe_3O_4, Fe_2O_3, SiO_2, TiO_2, etc [14-16] are available and reliable. Several factors [17], such as long-term stability [18, 19], thermal conductivity [20], viscosity [21], specific heat, and density [22], affect the heat transfer performance of nanofluids [8, 23, 24], as well as the structure of heat exchanger and the flow conditions.

Carbon-based nanoparticles such as carbon nanotubes, graphene oxide, and nanodiamond are reported to have promising high thermal conductivity [24-26]. Graphene (G) has attracted considerable attention due to the higher thermal conductivity of 5000 W/m.K, excellent electrical, mechanical, Young’s modulus, and optical characteristics [27]. Graphene has a 2D sheet-like structure similar to graphene oxide, but a significant difference is that graphene oxide has highly decorated carbon atoms. Reduced graphene oxide (rGO) is obtained by chemically modifying graphene oxide, and both are utilized as electrodes in lithium recharged batteries [28], adsorption substrates [29], whereas graphene oxide-based nanofluids are further used as heat transfer fluid because of high thermal conductivity. Said et al. [30] investigated carbon nanotubes/reduced graphene oxide-based hybrid nanofluids and examined thermophysical characteristics of the prepared nanofluids, using the fuzzy logic technique.

Hybrid nanofluids like graphene oxide-based cobalt oxide (Co_3O_4) nanocomposite can be promising with enhanced thermal conductivity and magnetic property [31]. These nanoparticles can be utilized in lithium-ion batteries [32], catalytic activity [33], and supercapacitor applications [34]. Furthermore, they can be used as heat transfer fluids [35]. Sajid and Ali [36] carefully reviewed the parameters which affected the hybrid nanofluids’ performance and observed that the most critical factor which affects thermal conductivity is the concentration of nanoparticles. Thermal conductivity enhancement for effective nanofluids is mostly accredited to higher surface area and high convection heat transfer within fluids, in addition to high Brownian motion. Toghraie et al. [37] investigated the effect of thermophysical properties of ZnO-TiO_2/EG hybrid nanofluids with respect to temperature (25-50 °C) and volume concentration (0-3.5 wt.%). Enhancement in thermal conductivity was observed by increasing either temperatures or volume concentration or both. Harandi et al. [38] observed a 30% enhancement in thermal conductivity of functionalized multiwalled carbon nanotubes (FMWCNTs)-Fe_3O_4/EG hybrid nanofluids at 2.3 wt.% concentration and 50°C. It was also observed that the temperature affecting thermal conductivity ratio was more noticeable with increased volume concentration. Afrand [39] examined the thermal conductivity of ethylene-glycol by adding nanoparticles of F-MWCNTs and magnesium oxide (MgO), and by changing temperature, and volume concentration range from 25 to 50°C and 0 to 0.6% respectively. They observed an improvement of 21.3% in thermal conductivity at 25°C and 0.6 wt.% volume concentration. Nine et al. [40] produced Al_2O_3-MWCNTs hybrid nanofluids to investigate thermal conductivity with volume concentration ranges from 1-6 wt.%. It was observed that spherically shaped nanoparticles had fewer enhancements in thermal conductivity as compared to cylindrically shaped nanoparticles in hybrid nanofluids. Esfahani et al. [41] investigated the effect of thermal conductivity of ZnO-Ag (50%- 50%)/H_2O nanofluids. Enhancement in thermal conductivity was noted as the Brownian motion became substantial by increasing volume concentration at high temperatures. Several other analyses on the effect of thermal conductivity on hybrid nanofluids are described further [8, 16, 30].

Soltani and Akbari [42] examined the impact of volume concentration and temperature on the viscosity of MgO-MWCNT/EG-based hybrid nanofluids. They observed a Newtonian behavior. They also observed that the dynamic viscosity displayed a declining trend with increasing temperature and volume concentration. Alirezaie et al. [43] investigated the effect of dynamic viscosity on COOH-FMWCNT's/MgO-engine oil hybrid nanofluids, and they observed a reduction with temperature. They also observed non-Newtonian behavior at a low temperature, which develops into Newtonian at high temperature. Zareie and Akbari [44] investigated the MgO-MWCNTs/H_2O-EG hybrid nanofluid to analyze the viscosity by varying temperatures from 25 to 50°C, and volume concentration ranges from 0.025 to 0.8 vol%. They reported enhancement in viscosity with an increase in particle loadings and an increase in temperature. Studies on the specific heat of hybrid nanofluids are reported in the literature: most of the studies showed a decreasing trend in the nanofluids with a rise in particle loadings and temperature [45-47]. For the reports presented on the density of hybrid nanofluids [48-50], the results showed an increase in density by increasing particle loadings and a decline in density by increasing the temperature. Adriana et al. [46] used a numerical approach to evaluate the thermal conductivity, viscosity and heat transfer characteristics of Al_2O_3, TiO_2, and SiO_2 hybrid nanofluids and they found thermal conductivity enhancement of 12% in addition to developing a new Nusselt number correlation. Bellos and Tzivanidis [47] prepared Al_2O_3 and TiO_2/Syltherm 800 hybrid nanofluids and estimated thermal efficiency by using hybrid nanofluids flow in parabolic trough collectors. They found a thermal efficiency enhancement of 1.8% and a Nusselt number enhancement of 178% using hybrid nanofluid.

The present research was carried out to understand the thermophysical characteristics of graphene-based cobalt oxide (Co_3O_4) hybrid nanofluids, which were synthesized in the laboratory, and water-based hybrid nanofluids that were produced and optimized using the ANFIS approach. The *in-situ*/chemical reduction technique was used to synthesize the rGO/Co_3O_4 nanocomposite and then characterized with x-ray diffraction, transmission electron microscope, and magnetometry. Experimental thermophysical properties such as thermal conductivity, viscosity, density, and specific heat were obtained at temperature values of 20, 30, 40, 50, and 60 °C and with particle loadings of 0.05%, 0.1%, and 0.2% wt.%. One of the main objectives of the current research work is to create a fuzzy model based on an experimental dataset for later use with optimization purposes to obtain the best operating conditions. A fuzzy system is one of the artificial intelligent (AI) tools that can accurately and efficiently model complex systems. The accuracy of using fuzzy logic technique in systems modelling is dependent upon its two main features. The first one is the nonlinear mapping between the inputs to the output of the fuzzy system through its rule-based list, and the second is the ability to learn through a training algorithm to update the fuzzy system's parameters. Based on the fuzzy model, the optimal control parameters can be determined. In this study, the objective is to determine the optimal (controlling) set of parameters that minimizes the density and viscosity but maximizes the thermal conductivity and the specific heat which represent the four controlled parameters. The controlling variables are temperature and percentage of nanofluid mixture. The experiments involve 20 input-output data samples that relate the controlled variables (outputs) to the controlling variables (inputs). The proposed strategy starts by building a robust model, and then applying the marine predators' algorithm (MPA) to determine the best set of input values that accomplish the goal of this study.

2. Materials and Methods

2.1. Synthesis of reduced graphene oxide (rGO)

Reduced graphene oxide (rGO) nanosheets were synthesized by a modified Hummers procedure [51].

Graphite powder of 2 g was mixed in 70 ml of concentrated sulphuric acid and 0.025 moles $NaNO_3$ for about 25 minutes, and then kept in an ice-water bath to cool down. The solution was mixed with 0.039 moles of potassium permanganate. The mixture was stirred for 20 minutes at 0^oC. The color of the solution changed to green because of the accessibility of the oxidizing agent (MnO^{3+}). The ice-water bath was removed, and distilled water of about 200 ml was added. Water was added to dilute the suspension and rinsed with 70 ml of hydrogen peroxide (H_2O_2) (30 wt.%) for half an hour to eliminate the contaminations. The mixture was centrifuged and rinsed various times with deionized water to remove sulphur. The rGO produced was dried at 60^oC in a vacuum chamber for 12 hours. To obtain carboxyl (COOH) groups on the surface of rGO, which was preserved with hydrochloric acid (HCL) for about 48 hours. The Co_3O_4 nanoparticles were attached to rGO's surface by carboxyl groups (COOH). The rGO nanomaterial was prepared in large quantities using the procedure mentioned above.

2.2. Synthesis of rGO/Co_3O_4

The synthesis procedure is displayed in **Fig. 1**. The rGO/Co_3O_4 hybrid nanomaterial was synthesized by in-situ/chemical reaction. First, 100 ml of water was added to 0.2 g of rGO in a 500 ml beaker and sonicated; in the meantime, 0.4 g of $CoCI_2.6H_2O$ was mixed with 40 ml of distilled water and stirred continuously. Both solutions were mixed and stirred slowly for up to 15 minutes, and then 0.2932 g of sodium borohydride was added, resulting in the formation of a black colour precipitate. The precipitate was rinsed with distilled water to eliminate sodium, chloride, and boron impurities and dried at 60^oC for one day. The same technique was used to prepare nanomaterials in a large quantity. Furthermore, pure Co_3O_4 nanoparticles were prepared for comparing results. The synthesized rGO/Co_3O_4 hybrid nanomaterial is shown in Fig. 1. Several characterization techniques were used to investigate the nanomaterial.

2.3. Characterization

Transmission electron microscopy (JEOL 2200F, 200KV) was used for the characterization of rGO and rGO/Co_3O_4 nanomaterial. Morphology and size of nanoparticles were estimated by using a transmission electron microscope (TEM). XRD (Siemens D-500) was used to obtain the patterns of rGO/Co_3O_4 and Co_3O_4. The VSM (Crogenics, UK) was used to obtain the magnetization of rGO/Co_3O_4 and Co_3O_4. The Fourier transform infrared (Bruker Equinox V70) was used to obtain the results of rGO/Co_3O_4, and Co_3O_4 nanoparticles.

2.4. Preparation of rGO/Co_3O_4 nanofluids

Particle loadings of 0.05 wt.%, 0.1 wt.%, and 0.2 wt.% were produced by diluting rGO/Co_3O_4. The physical properties of water, GO, Co_3O_4, and rGO/Co_3O_4 are presented in **Table 1**. A two-step method was employed to produce to rGO/Co_3O_4 nanofluids, using a probe sonicator. The production of nanoparticle preparation and suspension in a base fluid were processed individually in this method to reduce agglomeration and achieve better dispersion. This method is more dominant and efficient as compared to the one-step method. The prepared hybrid nanofluid sample is shown in **Fig. 1**. All the prepared nanofluid samples had pH values close to neutral (pH=6.5). Therefore, the prepared samples would not result in any corrosive reactions when used for a particular application.

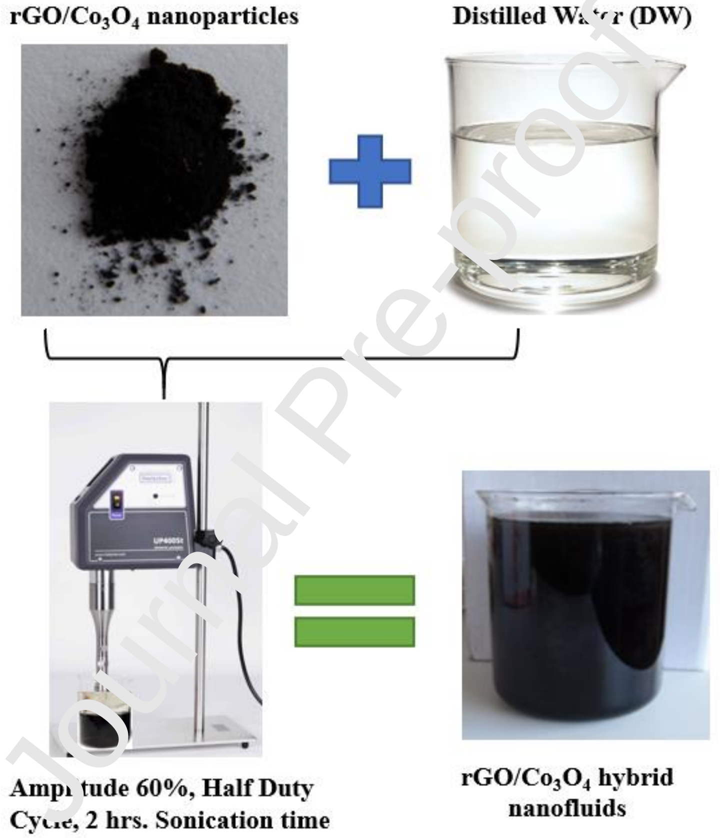

Fig. 1 (a) Synthesized dry rGO/Co_3O_4 nanoparticles suspended in distilled water to prepare rGO/Co_3O_4 hybrid nanofluids (0.2 vol. %) using probe sonicator.
The nanoparticles were suspended in the base fluid at pH=7.

Table 1: The properties of water, GO, Co_3O_4, and rGO/Co_3O_4 nanoparticles at 20°C.

Substance	ρ, (kg/m^3)	k, (W/m K)	C_p, (J/Kg K)	μ, (mPa.s)
Water	998.5	0.602	4178	0.89
GO	1910	1000	710	----

Co_3O_4	6110	69	460	----
GO/Co_3O_4	3296	692.7	627.5	----

2.4. Thermophysical properties

The thermal conductivity of hybrid nanofluids was characterized by the thermal conductivity (KD2 Pro, Decagon Devices Inc., USA). In the present study, thermal conductivity was measured by taking an average of 15 readings at 5-minute intervals with the help of a sensor KS1(~±5.0%). To stabilize the temperature, a water bath was used with 0.1°C accuracy. Measurements of viscosity were characterized by a sine-wave Vibro viscometer SV-10 (A&D Company, Japan) with ranges from 0.3 mPa.s to 10,000 mPa.s. Measurements were recorded and the average computed to consider final values with an interval of 5 K: a constant temperature bath controller was used to maintain the temperature. The flow behavior of samples was measured at different shear rates and temperatures.

The Archimedes' principle, the density was characterized by differential scanning calorimeter (DSC 2920 modulated, TA Instruments, New Castle, DE), and the specific heat was also measured. A controlled differential scanning calorimeter device was provided with a refrigerated cooling system (TA Instruments). The data was investigated using a Universal Analysis Program (Version 4.1D, TA Instruments). The cell constant was measured using indium and temperature, and enthalpy calibrations with indium, tin, and water as standards were performed. The aluminum sample pans (TA Instruments) were sonicated, first in methanol, and then in acetone, for 15 minutes each and air-dried before performing DSC experiments, and then the 10 mg solution was wrapped in an aluminum pan.

3. Modelling and Optimization

3.1 Adaptive Network-based Fuzzy Inference System (ANFIS)

Fuzzy logic (FL) appeared approximately in the 1960s. Since then its applications have been increasing day by day [30, 52]. Despite there being many types of research in the field of fuzzy logic, the structure of the fuzzy system remains the same. The structure comprises three main components, namely fuzzification, inference system, and defuzzification. The concept of fuzzy logic is considered as an expansion of the renowned Boolean logic. The latter deals with only two representations (0 and 1) of the events, but the former deals with multi-valued representations. Therefore, FL is thought to be much closer to human thinking. In binary systems, one may represent a case as either black or white, but definitely, there is something else in between. Thus, FL represents events, for example, black, grey, and white.

The output of the fuzzy system is obtained after three consequent operations have taken place. The first is to pass the crisp inputs to the fuzzifier to obtain the fuzzy value of the inputs. This process is done by mapping the inputs through fuzzy membership functions (MFs). The accessible fuzzifying functions are the Gaussian and triangular shapes. The fuzzified inputs are then passed to fire the fuzzy IF-THEN rules in order to obtain the rules' fuzzy outputs in the second component. Usually, the rule takes the form IF (*Antecedent*) THEN (*Consequence*). The *Antecedent* is a logical input combination; however, the *Consequence* is the rule's output. There are two famous structures (types) of fuzzy rule. In 1975, Mamdani proposed the first form of a fuzzy rule in the design of a controller to a heat transfer application. Ten years later, Sugeno and his colleagues revealed the second type. Equations (1) and (2), are examples of the rules of two-input one-output system for the Mamdani-form and the Sugeno-form, respectively.

$$\text{IF } a \text{ is } MF_a \text{ and } b \text{ is } MF_b \text{ THEN c is } MF_c \quad (1)$$

$$\text{IF } a \text{ is } MF_a \text{ and } b \text{ is } MF_b \text{ THEN c} = f(a, b) \quad (2)$$

where, a and b are the system's inputs with MF_a and MF_b as their fuzzy membership functions, respectively; c is the system's output, and MF_c is its fuzzy membership function; $f(a, b)$ is either a linear or nonlinear function of the two inputs a and b.

The fuzzy outputs of whole fired rules are aggregated to obtain one fuzzy output. Through the third component, the final fuzzy output is defuzzified to come up with the final crisp value of the output. In Mamdani-type form, the Centre of Gravity (COG) is the most suitable defuzzifier; however, the Weighted Average (Wavg) is more prevalent in the Sugeno-type. In the mid-nineties of the last century, Jang developed a fuzzy inference system (FIS) by means of an artificial neural network (ANN), namely the Adaptive Network-based Fuzzy Inference System (ANFIS). Consequently, the conjunction between the two strategies re-enforced the resulting system with the ability to model a complex system with high nonlinearity as well as to be trained in the same procedure as the one used in ANN.

3.2 MPA Optimizer

The marine predators algorithm (MPA) is a very new optimizer that was proposed by Faramarzi et al. in March 2020. The main MPA inspiration is the widespread search for food strategy, which is the movement of Levy and Browne among surrounding predators together with an optimum encounter of modified policy in the biological interface between the predator and the prey. More details about core idea and mathematical representation can be found in [53]. In MPA, the prey, as well as the predator, is viewed as search representative, since the predator is searching for the prey; meanwhile, the prey itself looking for its food. The velocity ratio among the predator and the prey is the key factor in transferring the process from one stage to another. In MPA, the large-velocity ratio is a notable feature in the first phase, whereas unity and low ratio are the visible markers for the second and third stages.

The optimization process by MPA contains three main stages dependent upon the speed ratio between the prey as well as predator. In the first stage (high ratio) the prey moves very fast searching for its food; meanwhile, the predator stands without moving. This situation occurs in the first third of repetitions when the step size or the velocity is large for high evaluation ability. The step size in this stage can be formulated by the following relation [53];

$$S_{size} = R_B \otimes \left(\overrightarrow{Elite}_i - R_B \otimes \overrightarrow{\mathrm{Prey}}_{\mathrm{i}} \right) \tag{3}$$

Where;

$\overrightarrow{Elite}$ denotes the fittest solution which is nominated as the top predator

$\overrightarrow{\mathrm{Prey}}$ represents another matrix with a similar dimension as $\overrightarrow{Elite}$ where the predators review their positions based on it.

R_B is a random vector

$\otimes$ denotes the process of eliminating wise multiplications.

For the second phase, both the predator and the prey are shifting at the same velocity. This stage occurs in the middle stage of the optimization procedure. Accordingly, part of the population is nominated for investigation and the other half for utilizations. The prey is accountable for utilization and the predator for investigation. The prey moves in Lévy, whereas the predator moves in Brownian.

The step size for the first half of the population can be estimated as follows;

$$S_{size} = R_L \otimes \left(\overrightarrow{Elite}_i - R_L \otimes \overrightarrow{\mathrm{Prey}}_{\mathrm{i}} \right) \tag{4}$$

Where R_L is a vector of random numbers founded on Lévy's distribution

The second half of the population follows the Brownian strategy. In the last stage, the predator is moving quicker than the prey. This stage occurs at the end of the optimization procedure, which is typically related to great exploitation ability. Therefore, the Lévy distribution is adopted to update the step size of the population.

Based on the developed fuzzy models, the MPA optimizer is applied to obtain the optimal values of the controlling parameters (i.e., temperature and nanofluid mixture percentage) that minimize two controlled variables (i.e., density and viscosity) as well as maximize the other two controlled variables (thermal conductivity and specific heat). In this study, the optimization procedure is done in two different strategies. The first is to optimize each output individually as a single-objective (SO) function. The second is to optimize the whole set of outputs all at once (simultaneously). The latter procedure could be considered as a multi-objective (MO) optimization. However, the MO optimization can be transformed to be manipulated as a SO by summing up the normalized SO functions, as shown in Equation (3).

$$f(X) = WY^{\mathrm{T}} \tag{3}$$

where, $X = [x_1, x_2]$, $W = [w_1, w_2, -w_3, -w_4]$ and $Y = [\, y_1, y_2, y_3, y_4]$

X is the controlling variables' vector that refers to the temperature and the nanofluid mixture's percentage, respectively; W is the scaling (normalizing) vector, which is equal to [1002, 1.50263, -0.778, -4183] and Y is the output's vector that refers to the density, viscosity, thermal conductivity, and specific heat, respectively.

4. Results and Discussion

4.1. Characterization of rGO/Co_3O_4

The TEM (JEOL 2200F, 200KV) results were presented in **Fig. 2b** and the TEM samples were prepared by water diluted rGO/Co_3O_4 deposited on the copper grid. Results clearly indicated the synthesized rGO is a 2-dimensional sheet (left-side image) without any impurities. Based on the in-situ growth technique, the cobalt oxide is reduced onto the rGO sheet through –COOH groups, and these –COOH groups act as a covalent bond between rGO and Co_3O_4 and help with the uniform dispersion of nanoparticles in water. The TEM results of rGO/Co_3O_4 clearly show the Co_3O_4 nanoparticles are dispersed on the top surface of the rGO sheet.

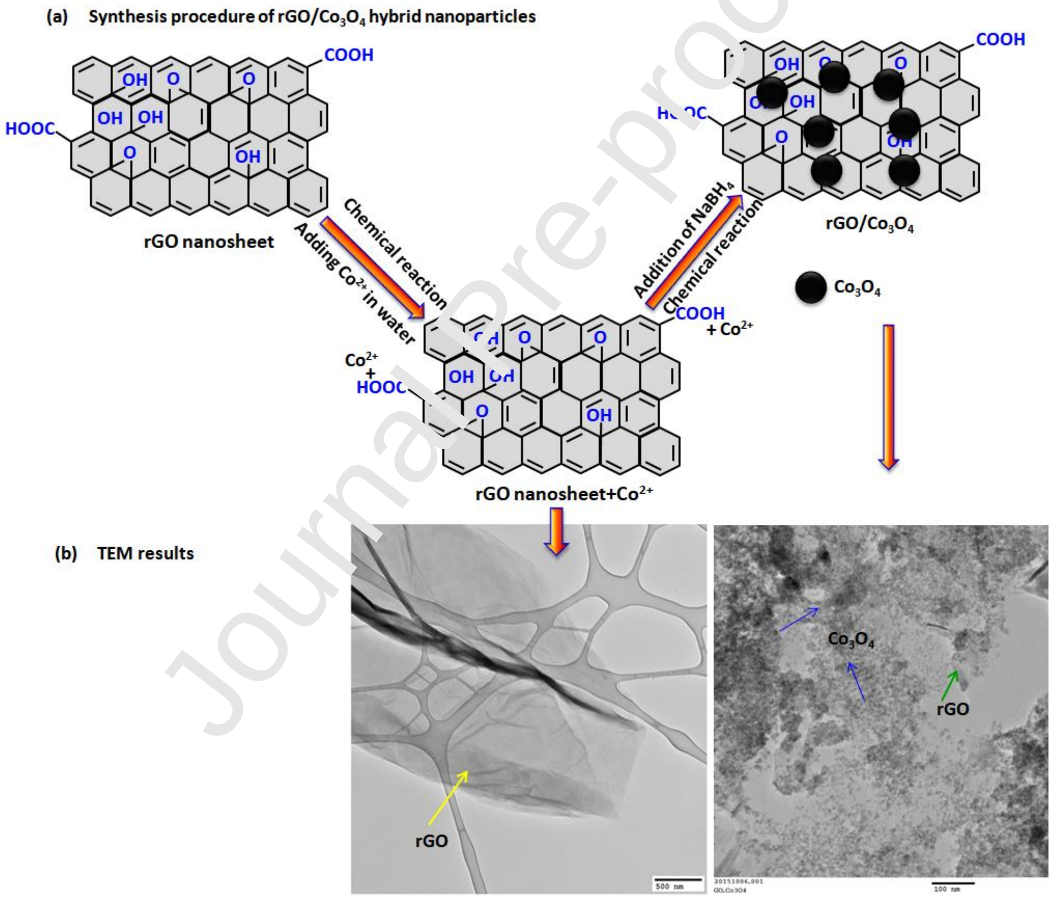

Fig. 2 rGO/Co_3O_4 hybrid nanoparticles, (a) synthesis procedure, and (b) TEM results

The Fourier transform infrared (Bruker Equinox V70) spectra rGO, Co_3O_4, and rGO/Co_3O_4 are indicated in **Fig. 3**. The IR spectra of rGO indicate the presence of various groups: the wavenumbers of 1623 cm^{-1} and 1726 cm^{-1} indicate the C=C group and C=O groups. These two groups reveal the formation of –COOH groups on the surface of rGO. Additionally, the wavenumber of 1044 cm^{-1}, 1221 $cm^{-1,}$ and

1411 cm^{-1} indicated the formation of C–O–C epoxy or alkoxy groups. The IR spectra of Co_3O_4 also presents various groups: the wavenumbers of 584 cm^{-1} and 671 cm^{-1} are related to the Co–O vibration [54], which shows that Co^{2+} is oxidized into Co_3O_4. Moreover, the IR spectra of rGO/Co_3O_4 exhibits the peaks of both rGO and CO_3O_4, which are at wavenumbers of 1623, 1726, 1044, 1221, and 1411 cm^{-1} related to C=C, C=O, and C–O–C groups for rGO and the wavenumbers 584 and 671 cm^{-1} are related to Co–O groups for Co_3O_4.

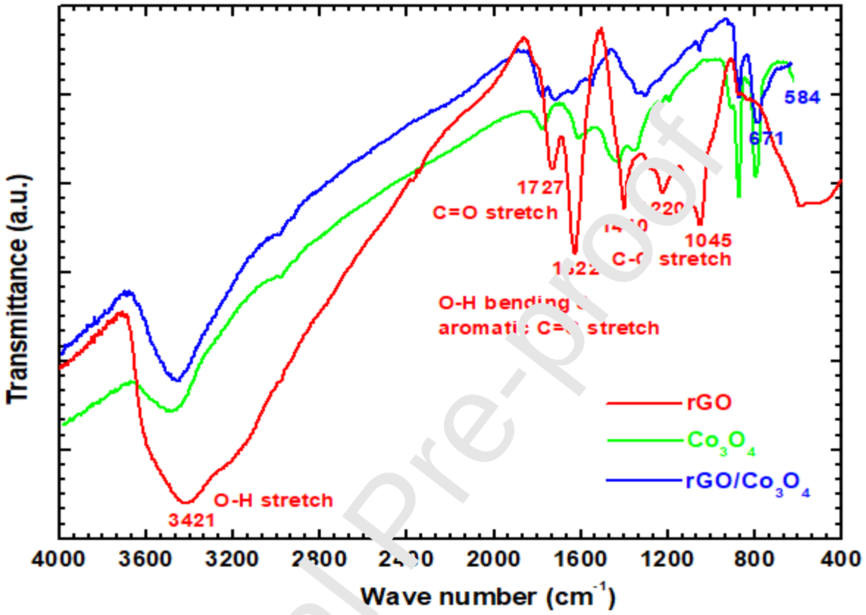

Fig. 3 FTIR results of the prepared nanomaterials.

The XRD (Siemens D-500) patterns of rGO/Co_3O_4 and Co_3O_4 are represented in **Fig. 4.** From the XRD pattern, the Co_3O_4 nanoparticles planes of (111), (220), (311), (400), (511), and (440) and the corresponding 2θ positions of19.03°, 31.31°, 36.87°, 44.81°, 59.42°, and 65.25° were perfectly matched with the JCPDS card No. 073-1701 file, which identifies the cubic structure of the nanoparticles. The rGO plane of (002) and the corresponding 2θ position is 11.67°, which can be observed in the rGO/Co_3O_4 nanoparticles, and it is marked in the figure.

The average hybrid nanoparticle size was evaluated based on Scherrer's expression proposed by Sundar et al. [55], and the equation is presented below.

$$\text{Scherrer's equation, } \delta = \frac{0.94\,\lambda}{B(2\theta)Cos\theta} \tag{1}$$

The terms in Eq. (1) are particle size (δ), Bragg angle (θ), and wavelength (λ =1.5405 Å) and $B(2\theta)$ is the peak at full width half maximum.

From XRD patterns, the $B(2\theta)$ value is 1.3° (0.0226 radians) and (θ) = 36.83°. By substituting these values in Eq. (1), it was found that the hybrid nanoparticle size is 79.64 nm.

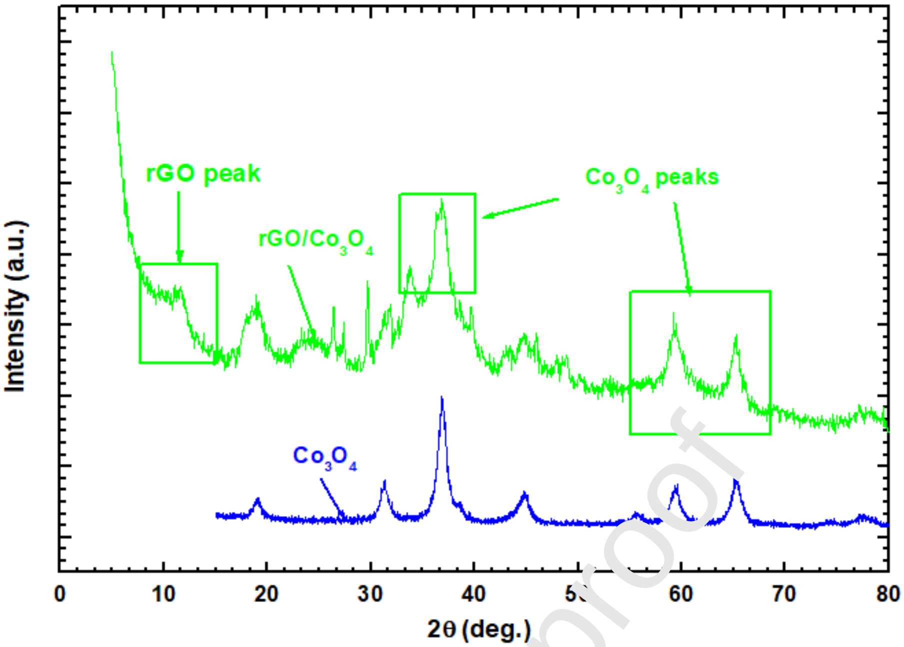

Fig. 4 XRD results of the prepared nanomaterials.

The weight composition of rGO and Co_3O_4 nanoparticles was analyzed on the magnetic characterization. The composite matrix contains non-magnetic material (rGO) and magnetic material (Co_3O_4). The same synthesis procedure is adopted without using rGO for the preparation of Co_3O_4 nanoparticles for comparison purposes. **Fig. 5** shows the magnetic (Crogenics, UK) results of both rGO/Co_3O_4 and Co_3O_4. By using rGO, the magnetic behaviour of Co_3O_4 is decreased. The magnetization value of Co_3O_4 is 14.23 emu/g [56, 57], but with the mixing of rGO its value is decreased to 4.67 emu/g. Based on the magnetization rule, the decreased magnetization of Co_3O4 is 33%, which means 67% of rGO is present in the rGO/Co_3O_4 material matrix. Fig. 5 shows the magnetic measurement results, which indicate the potential of the prepared hybrid nanoparticles to be used as ferrofluids, due to their magnetic property.

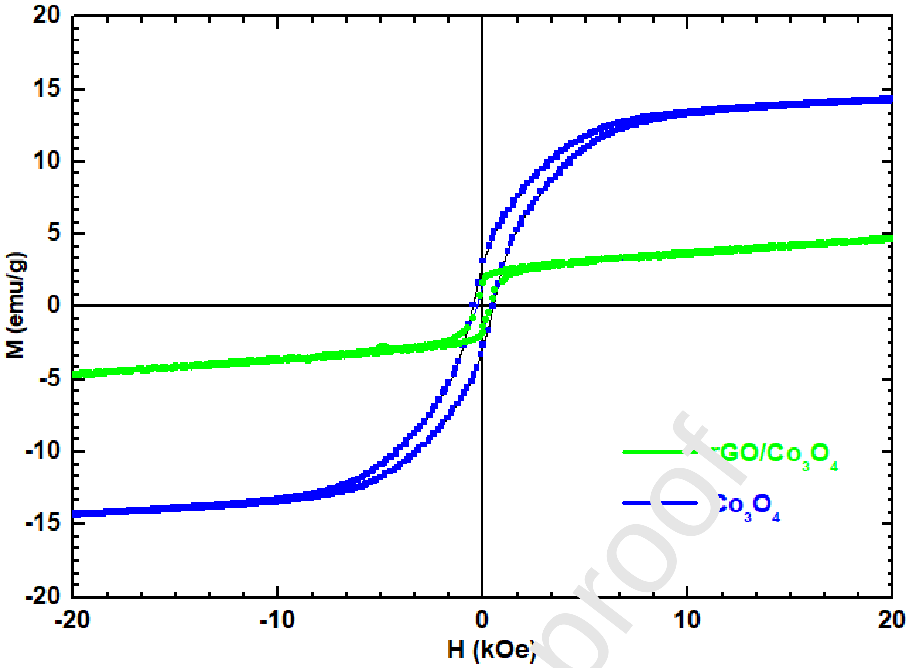

Fig. 5 Magnetic measurement results of the prepared nanomaterials.

4.2. Thermophysical properties of rGO/Co$_3$O$_4$ nanofluids

The properties of thermal conductivity, viscosity, density, and specific heat are measured for heat transfer and thermal performance applications with the weight concentrations of 0.05%, 0.1% and 0.3% for temperatures from 20°C to 60°C.

4.2.1. Thermal conductivity and viscosity of nanofluids

The most complex and essential thermophysical property of nanofluids is thermal conductivity, which has attracted attention from researchers. There are some factors such as the concentration of nanoparticles, base fluid, temperature, particle size, Brownian motion of particles, clustering effect, and pH value that impact the thermal conductivity of hybrid nanofluids.

In the study, the thermal conductivity and viscosity of hybrid nanofluids were measured experimentally, and the data is recorded in Fig. 6 and Fig. 7, respectively. By increasing the particle loading wt.% and temperature, enhancement in thermal conductivity was observed. The enhancement in thermal conductivity of 2.82%, 3.82%, and 7.64% was observed at 20°C and 0.05 wt.%, 0.1 wt.%, and 0.2 wt.%, respectively, as compared to water data. At 60°C, the enhancement in thermal conductivity was 8.58%, 12.40%, and 19.14%, respectively, as compared to water data, as presented in Fig. 6. Intensifying the temperature increases the kinetic energy, and the interface, because of more significant Brownian motion, is improved, which in turn increases thermal conductivity. The increase in particle loading not only results in higher thermal conductivity and viscosity, but also causes aggregations, which make the performance susceptible [58, 59]. The cluster formations of the investigated hybrid nanofluid could be a possible mechanism for enhanced thermal conductivity. An increase in thermal conductivity with the increase in temperature is desirable for applications that work at higher temperatures.

The modification in the pH value of the hybrid nanofluids provides effective outcomes to enhance the thermal conductivity. Optimum pH value signifies enhanced dispersion of nanoparticles in the base fluid due to the improved electrostatic repulsive forces that reduce clusters and improve performance. The nanoparticle size has a significant impact on the thermal conductivity of nanofluids. Most literature has reported the effect of nanoparticle size on thermal conductivity enhancement. It was observed that smaller nanoparticles provided high thermal conductivity as compared to large-sized nanoparticles. The effect of sonication might also play a significant role in the enhancement of thermal conductivity. All these parameters should be taken into account to enhance the thermal conductivity of hybrid nanofluids [60].

It was observed by increasing particle loading wt.% that the viscosity improved, but it decreased with a rise in temperature as presented in Fig. 7. The viscosity was enhanced up to 7.59%, 16.45%, and 49.39% at 0.05 wt. %, 0.1 wt.%, 0.2 wt.% at 20^{o}C, whereas at 60^{o}C, the enhancement was observed at about 16.66%, 33.33% and 70.83%, respectively as compared to water data. The enhancement in the viscosity of hybrid nanofluids is due to the high resistance among the fluid layers and the high density of nanoparticles [61, 62]. The variation in viscosity affects the flow property parameters such as pumping power, convective heat transfer, and pressure drop. Van der Waals forces became noteworthy by increasing the particle concentration, which caused nanoclusters. These clusters opposed the fluid's movement and thus enhanced viscosity. The impact of increasing the volume concentration was significant at low temperatures as compared to high temperature, where the Van der Waals forces at high temperature are lower. Conclusively, the interaction between the molecules of the base fluid and the nanoparticles, as well as adhesive intermolecular forces among the particles, results in an increase of viscosity for the studied hybrid nanofluids.

Several investigations examined the effects of various parameters such as particle size, stability, sonication time, temperature, particle concentration, and the dispersion methods on the conventional nanofluids' viscosity [63]. Most literature focused on the impact of temperature and volume concentration with several nanoparticles in hybrid nanofluids. These are the parameters that affect viscosity the most, but other parameters are also significant. Scholars in the future should conduct studies, taking these parameters into consideration, to improve and analyze the models for precise computation of viscosity.

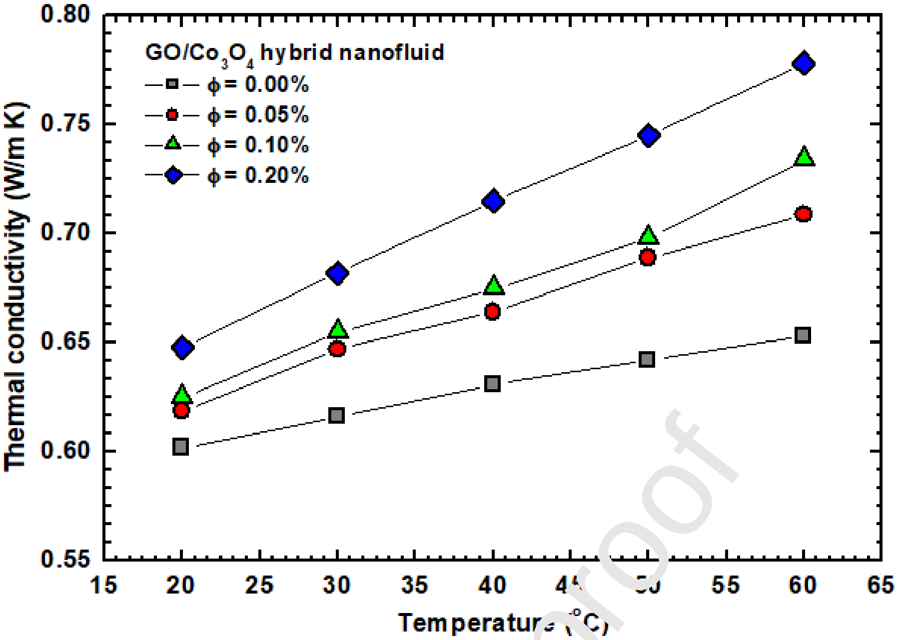

Fig. 6 Thermal conductivity for different concentrations and changing temperatures.

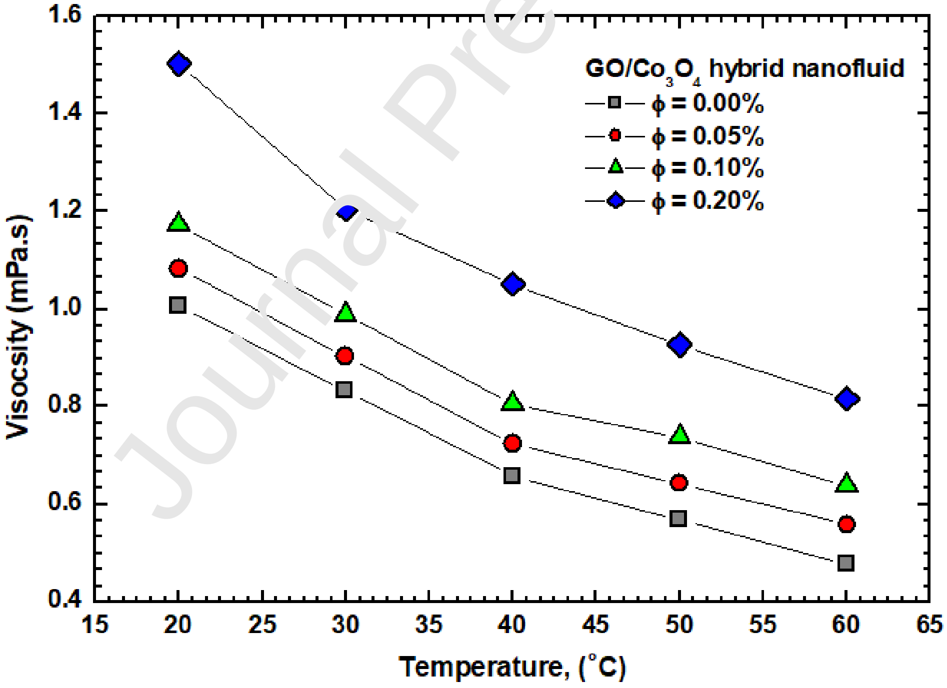

Fig. 7 Viscosity for different concentrations and changing temperatures.

4.2.2. Density and specific heat of nanofluids

The Archimedes' principle, the density of nanofluids were measured, and a differential scanning calorimeter was used to measure the specific heat of nanofluids, the data for which is presented in Fig. 8 and Fig. 9, respectively. With increased particle loadings, the density increased, but it decreased with the increasing temperatures. At 0.05%, 0.1%, and 0.2% particle loading wt.%, the density rise was 1.0011-times, 1.0022-times, and 1.0045-times at 20°C; simultaneously, the density rise was 1.0012-times, 1.0023-times and 1.0047-times at 60°C, respectively compared to water data as shown in Fig. 8. Due to particle loadings in the base fluid, the mass of the fluid increased. The increment in the density of the hybrid nanofluids is due to the density of nanoparticles, which is more significant compared to the base fluid, which attributes the interface effects of the bulk fluid properties, as well as the interaction between the nanoparticles [64].

The specific heat of nanofluids decreased with increased particle loadings and temperatures. At 0.2 wt.%, the maximum decreased specific heat is 0.192% and 0.194% at 20°C and 60°C, when compared with water, but no effect was observed with the increase in temperature; however, a similar trend as of the water was followed, which is shown in Fig. 9. Under the fixed heat supplied to base fluid and nanofluids, the temperature difference is lower for nanofluids compared to water. The specific heat of the hybrid nanofluids decreased with the increase in the concentration of the nanoparticles and the same pattern as that of the base fluid was followed with the increase in temperature. This could possibly be explained that due to the higher surface area of the hybrid nanoparticles, the more significant impact of the surface free energy on the overall specific heat capacity. Very few studies [45-47], have been reported in the literature on the specific heat capacity of hybrid nanofluids and these studies showed a similar trend as observed for our samples.

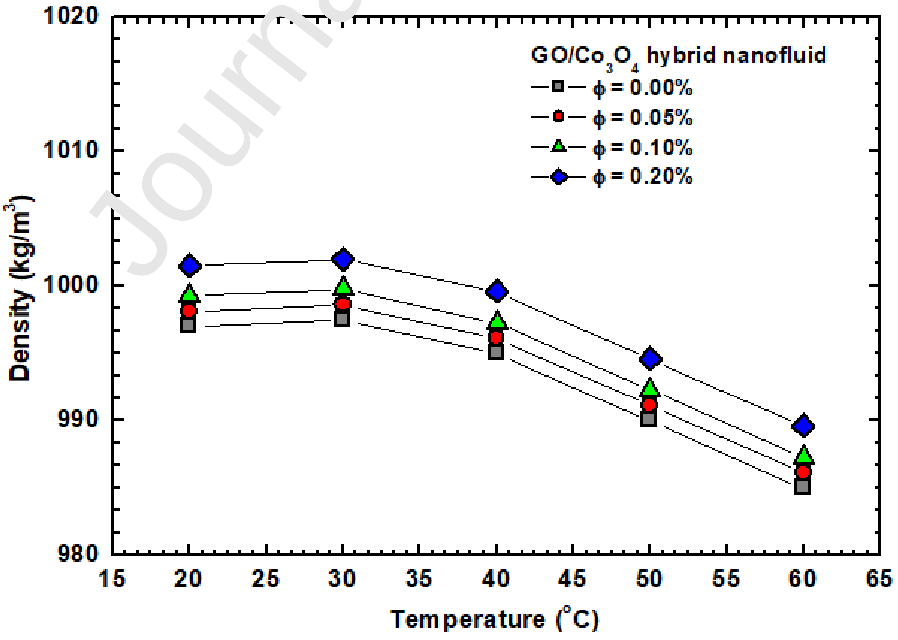

Fig. 8 Density for different concentrations and changing temperatures.

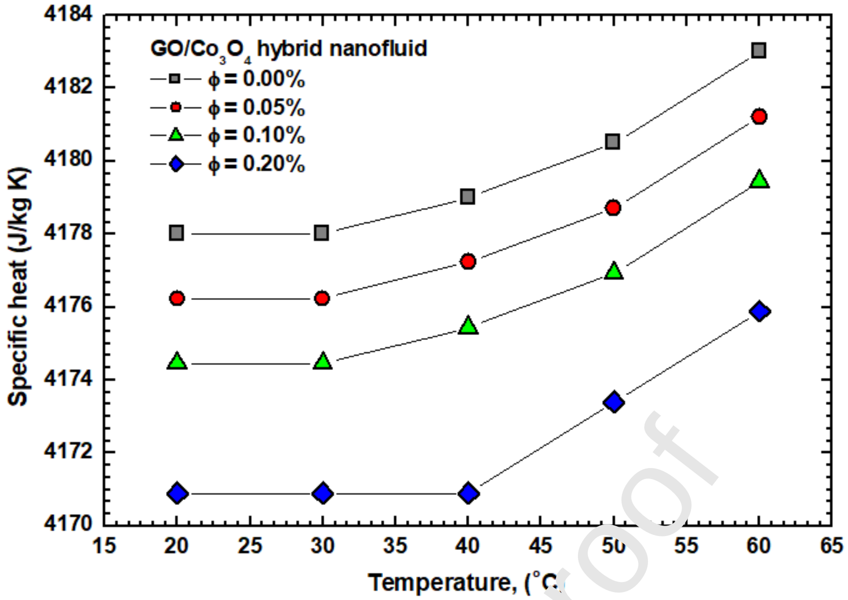

Fig. 9 Specific heat of different particle loadings of hybrid nanofluids at different temperatures.

4.3 Modeling and optimization

4.3.1 ANFIS-based Modelling

Systems modeling is a strategy often used in engineering applications in two main instances. The first is to predict output for inputs that have values different from those conducted in the experiments, but the values are within the input-space. The second is to predict output for inputs that have values beyond the input-space. In both cases, the resulting model must be robust as well as accurate for it to be relied upon. Modelling using ANFIS strategy proved to be an efficient tool, especially in complex and nonlinear systems.

In this study, only 20 data samples were available. Each of them represents a case where the temperature and volume concentration of nanoparticles take a value of 20, 40, 50, and 60°C and 0, 0.05, 0.1, and 0.2, respectively. The dataset was divided into two subsets. The first subset comprised of 75% (15 samples) of the data samples and was assigned to training. The remaining 25% (5 samples) was assigned for testing. The testing subset is usually used to guarantee the success of the training phase and ensure those model predictions are accurate and trustable. The fuzzy system's structure is Sugeno-type, which is the most appropriate one for modelling. The fuzzifying MF was selected in Gaussian shape, and the defuzzifying method was the Wavg. As the ANFIS is only applicable to a single output system, four ANFISes were constructed with a two-input one-output structure. Each ANFIS model represents one of the considered outputs. The fuzzy rules were formulated using the "Subtractive Clustering" (SC) algorithm. This algorithm can generate the rules from the input-output dataset with a minimum number of rules based on a clustering technique. The proposed models of density, viscosity, thermal conductivity, and specific heat ended up with a value of 7, 5, 7, and 5, respectively. All models were trained with 10 epochs, and the output function was 'linear'.

To examine the models' accuracies, every model was trained until a satisfying small value of the mean squared errors (MSE) for the testing subset were met. Table 2 summarizes the statistical measures of the modelling phase. The table shows the lowest MSEs values found so far from the training, validating, and entire data for the four models. The error here is considered as the difference between the experimental output and the fuzzy prediction. Also, the R^2 measure is an indicator of the well-correlation between the models' predictions and the experimental data, not only for the training subsets but also for the testing subsets where the values exceed 99%.

Table 2: The MSEs of the four fuzzy models' predictions for training, testing, and whole data

MSE / **Output**	**MSE**			**RMSE**			***R^2***		
	Train	**Test**	**All**	**Train**	**Test**	**All**	**Train**	**Test**	**All**
Density	1.26e-04	5.47e-02	1.38e-02	1.12e-02	2.34e-01	1.17e-01	1.0000	0.9986	0.9995
Viscosity	9.34e-09	8.36e-05	2.09e-05	9.67e-05	9.14e-03	4.57e-03	1.0000	0.9989	0.9997
Thermal Conductivity	1.43e-11	1.35e-05	3.39e-06	3.78e-06	3.68e-03	1.84e-03	1.0000	0.9957	0.9987
Specific Heat	1.30e-03	1.04e-01	2.71e-02	3.60e-02	3.23e-01	1.65e-01	0.9999	0.9977	0.9980

For a simple comparison between the fuzzy model computations and the experimental data, the visual plots are considered the easiest way. Therefore, the ANFISes outputs are plotted against the experimental values for the density, viscosity, thermal conductivity, and specific heat experimental datasets, respectively. The four models' outputs are plotted against the two inputs in a Three-Dimensional (3D) shape, as shown in figures (9a), (9b), (9c) and (9d). The plots are for both training and testing. From the figures, the predictions coincide well with the corresponding experimental data, which supports the correctness of the modelling phase.

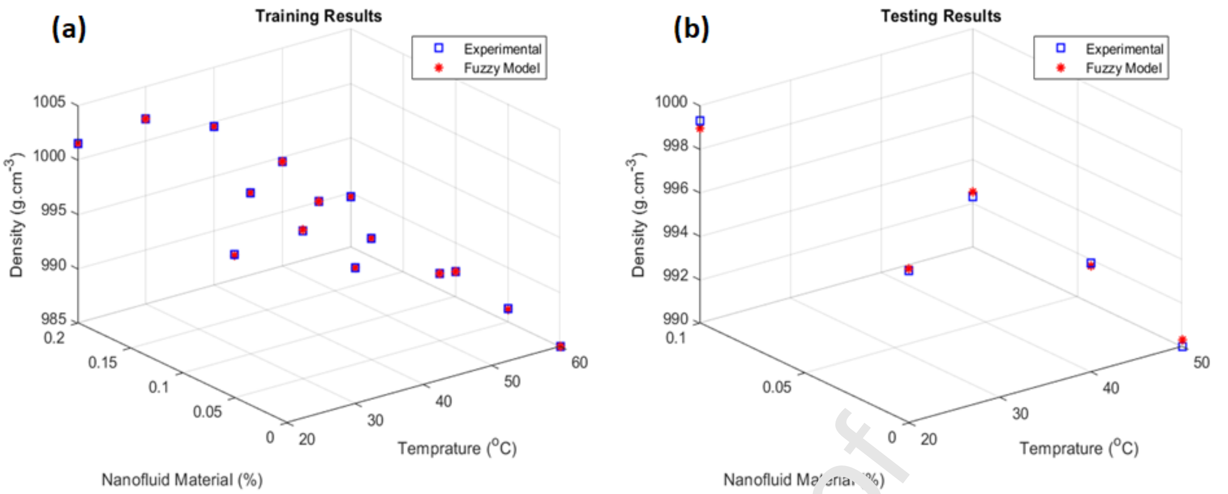

Fig. 9a A comparison between the experimental data and the outputs of the density's fuzzy model of a) training b) testing.

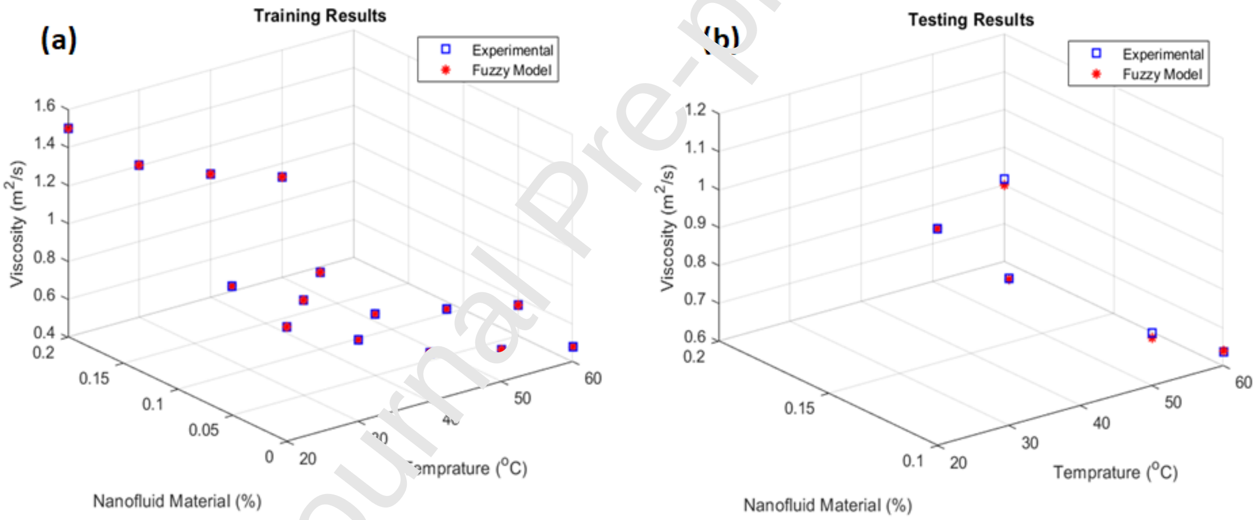

Fig. 9b. A comparison between the experimental data and the outputs of the viscosity fuzzy model of a) training b) testing.

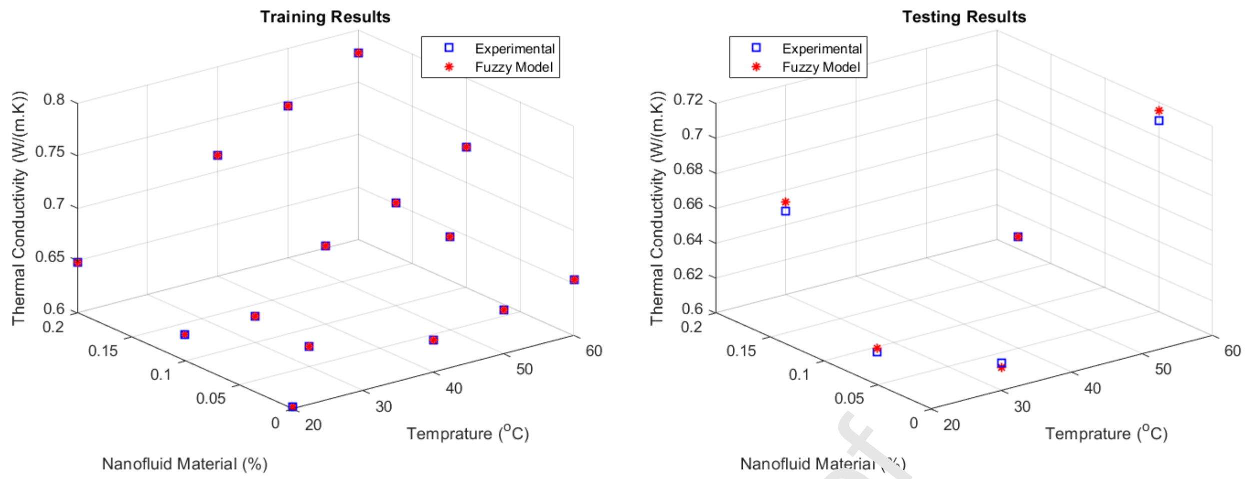

(a) (b)

Fig. 9c. A comparison between the experimental data and the outputs of the thermal conductivity fuzzy model of a) training b) testing.

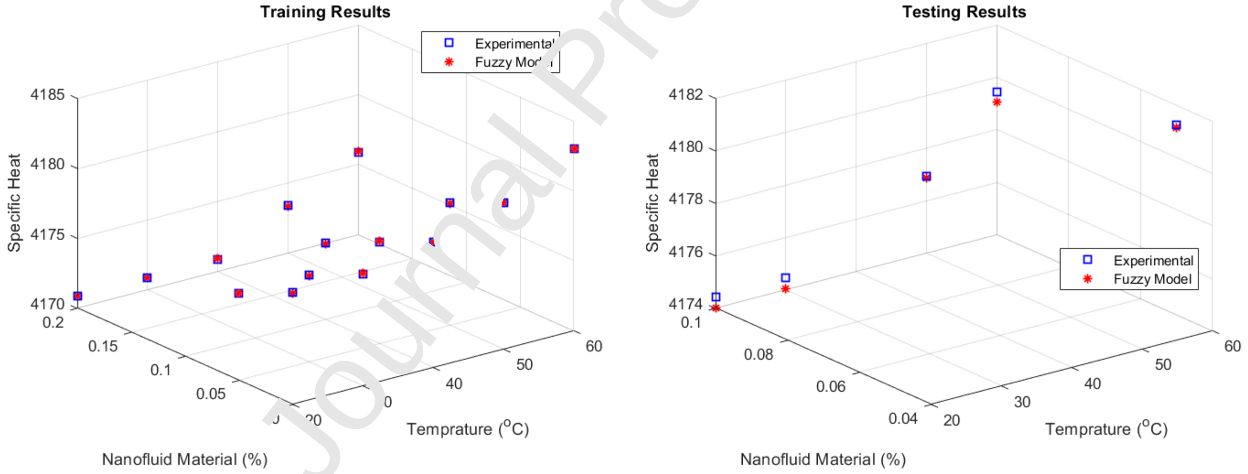

(a) (b)

Fig. 9d. A comparison between the experimental data and the outputs of the specific heat's fuzzy model of a) training b) testing.

In modelling, the visualization of the spatial shape helps in understanding the relationship between the inputs and the output. Figures (10a), (10b), (10c) and (10d) show the 3D shape with the contours of the ANFISes models, respectively. The contour curves are helpful in illustrating the nonlinear behavior of the output in terms of the variation of the inputs.

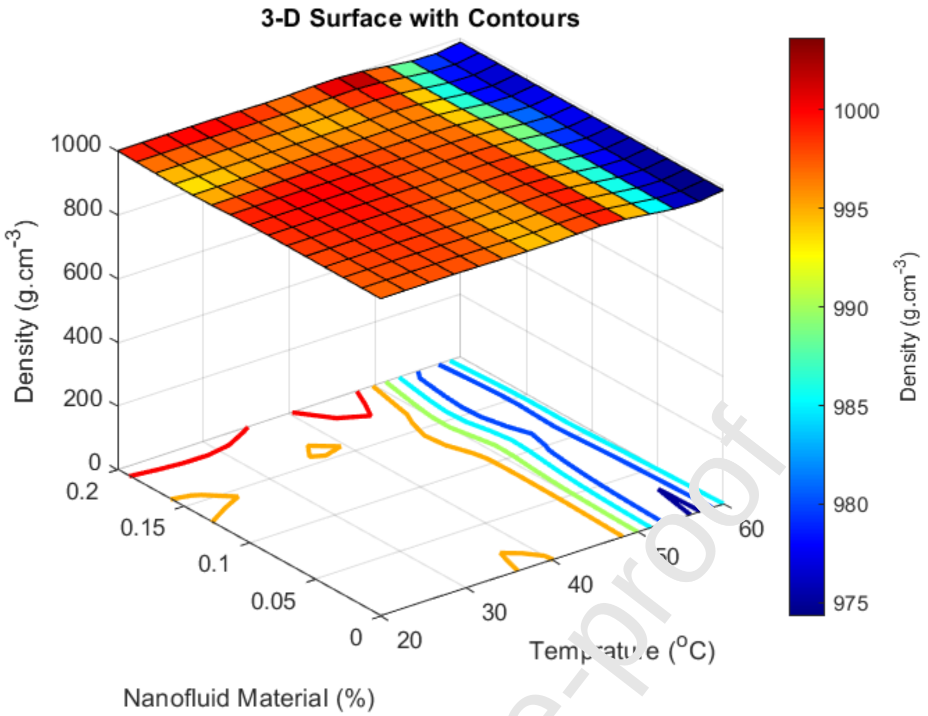

Fig. 10a. The 3-D spatial shape that relates the density with temperature and nanofluid material.

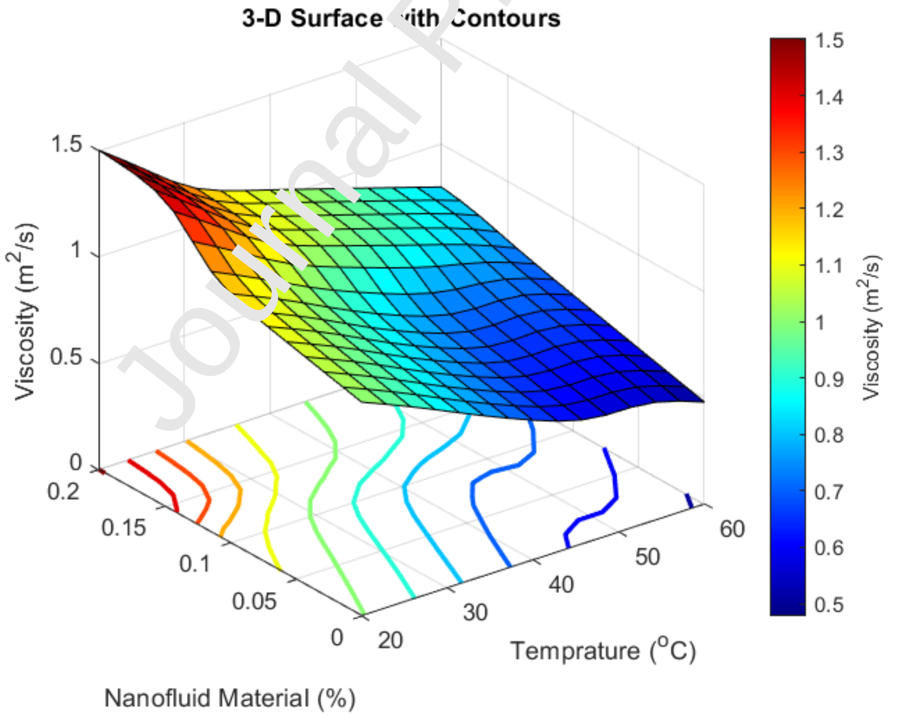

Fig. 10b. The 3-D spatial shape that relates the viscosity with temperature and nanofluid material

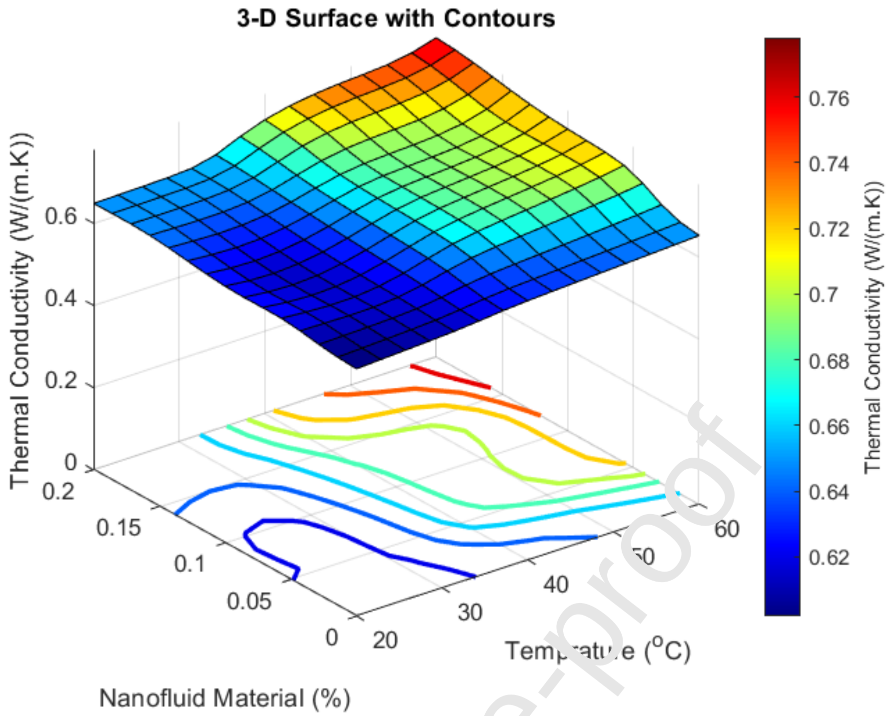

Fig. 10c. The 3-D spatial shape that relates the thermal conductivity with temperature and nanofluid material

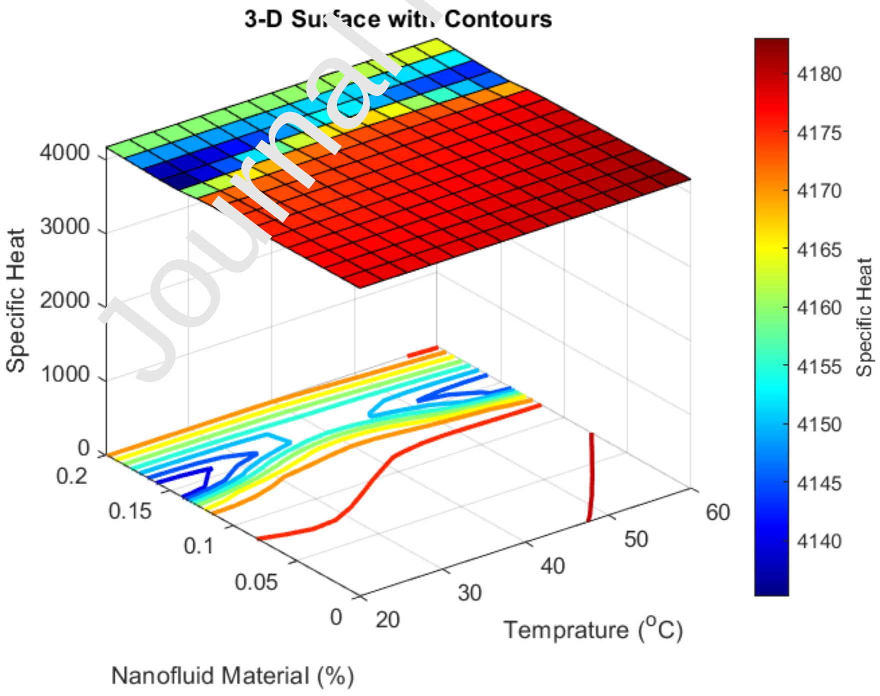

Fig. 10d. The 3-D spatial shape that relates the specific heat with temperature and nanofluid material

The resulting Gaussian membership functions for the temperature and nanofluid mixture after applying the SC method and the 10 epochs training phase are shown in figures (11a), (11b), (11c) and (11d) for density, viscosity, thermal conductivity, and specific heat, respectively.

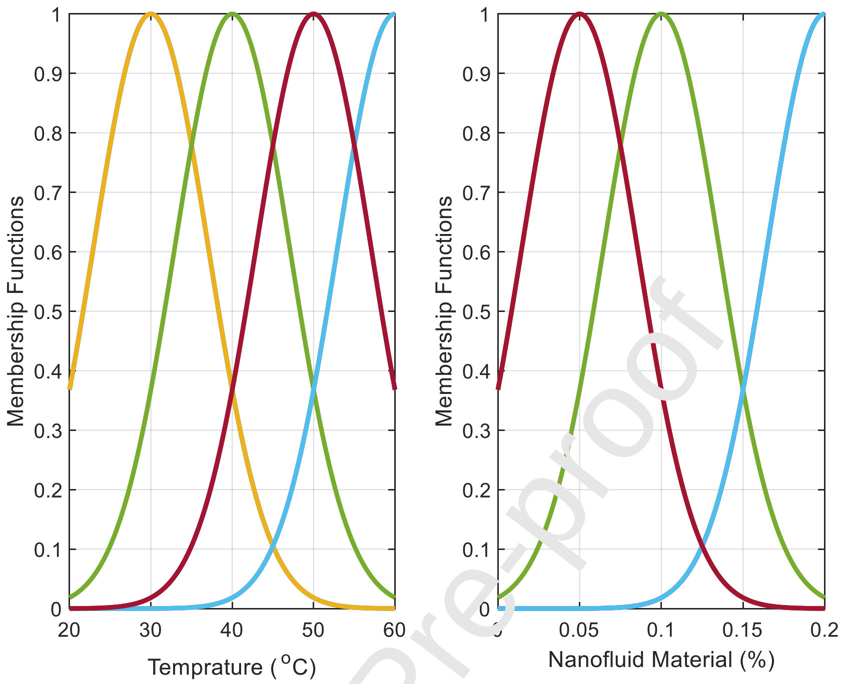

Fig. 11a. The density fuzzy model inputs’ MFs.

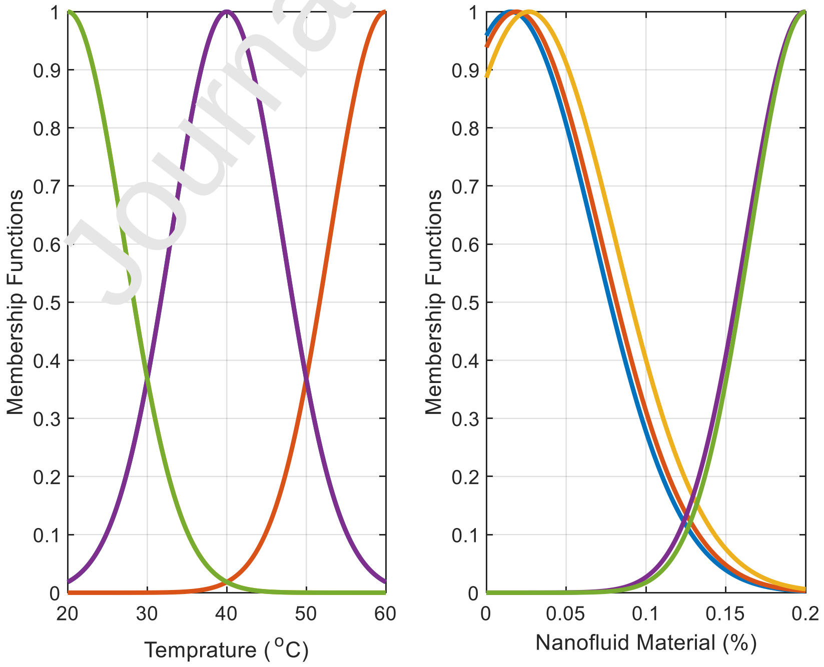

Fig. 11b. The viscosity fuzzy model inputs’ MFs.

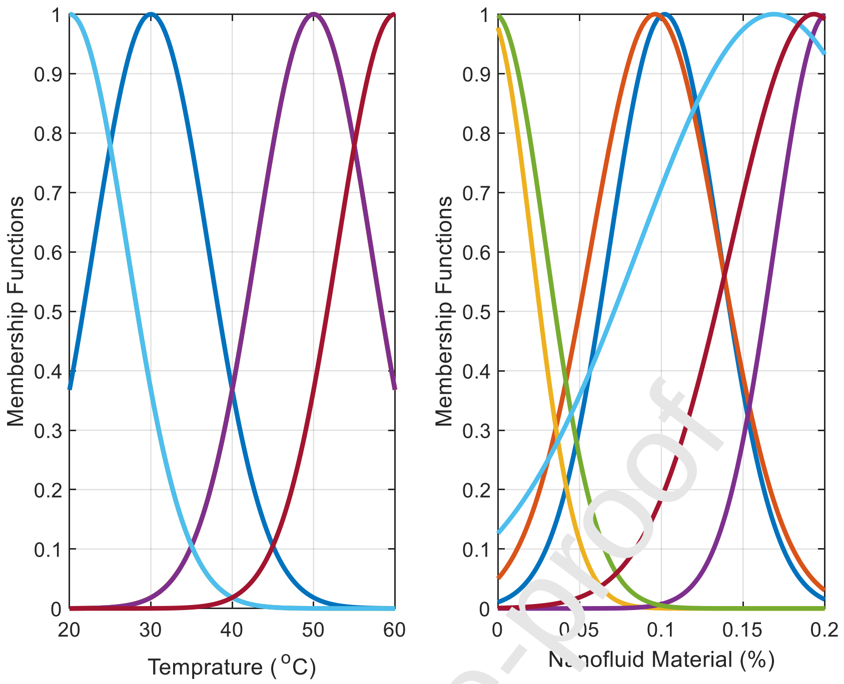

Fig. 11c. The thermal conductivity fuzzy model inputs' MFs.

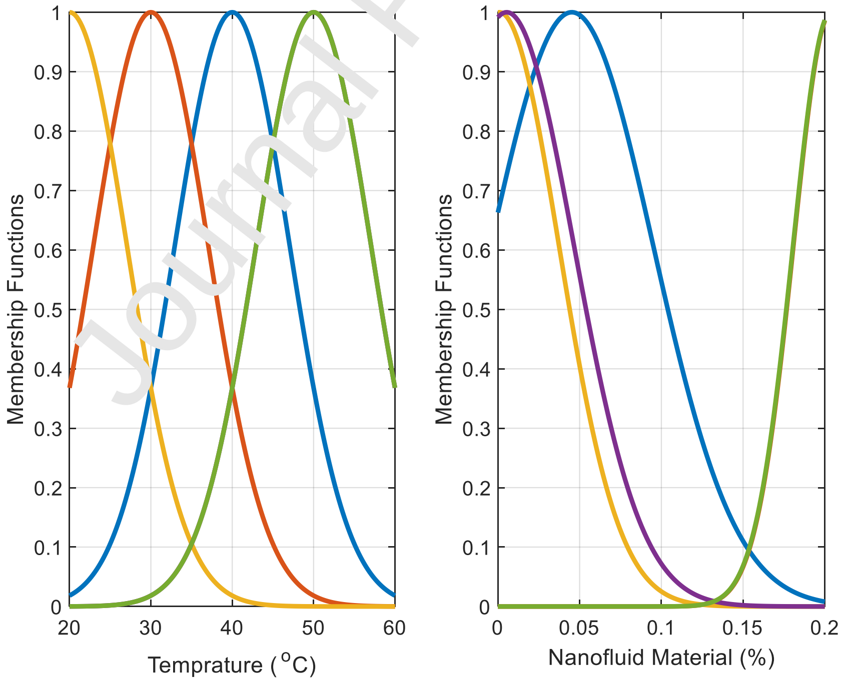

Fig. 11d. Specific heat fuzzy analysis inputs' MFs.

Usually, the prediction accuracy plot is mandatory to measure the extent to which the model predictions are trustable. Therefore, the predicted data are plotted against the target data for the training as well as the testing subsets. These plots for the four models are shown in figures (12a), (12b), (12c), and (12d), respectively. It can be clearly noticed that the predictions in the figures are close to one hundred percent accuracy, which is represented by the diagonal line.

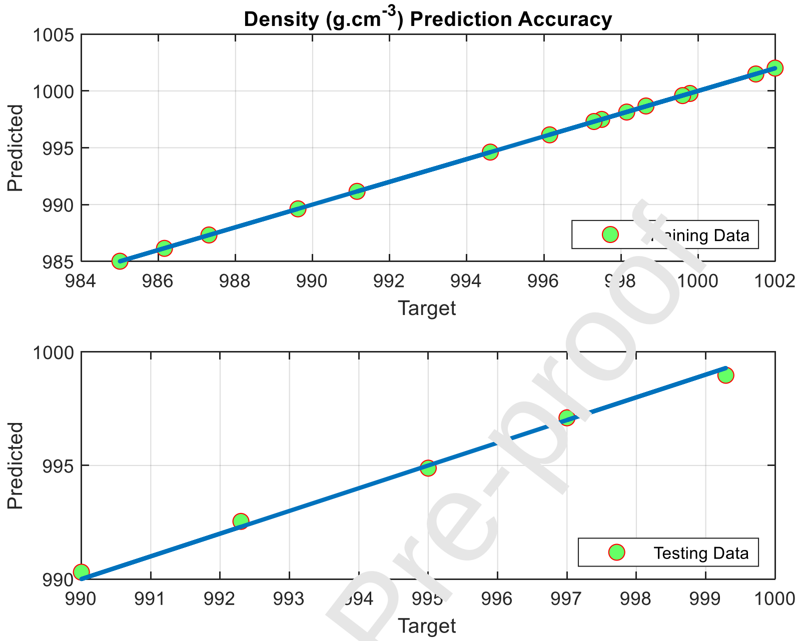

Fig.12a. Density fuzzy analysis prediction accuracy.

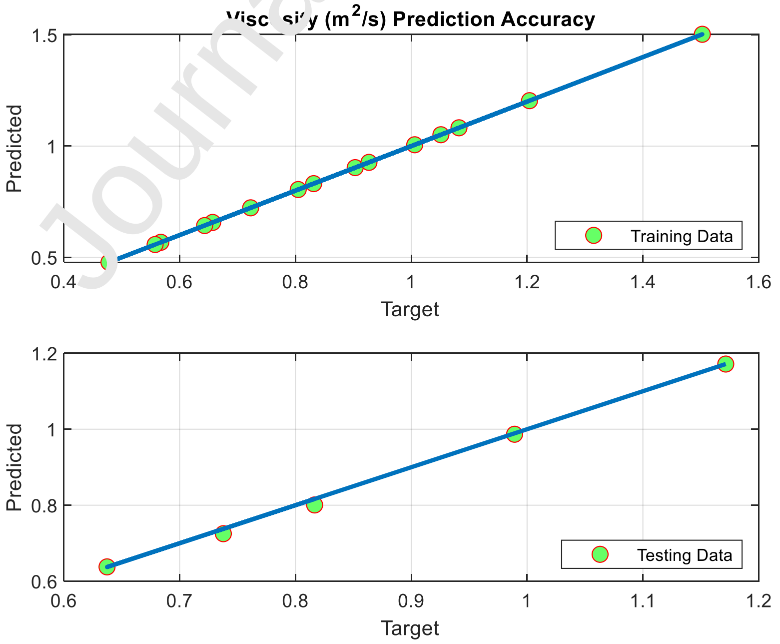

Fig12b. The viscosity’s fuzzy analysis prediction accuracy

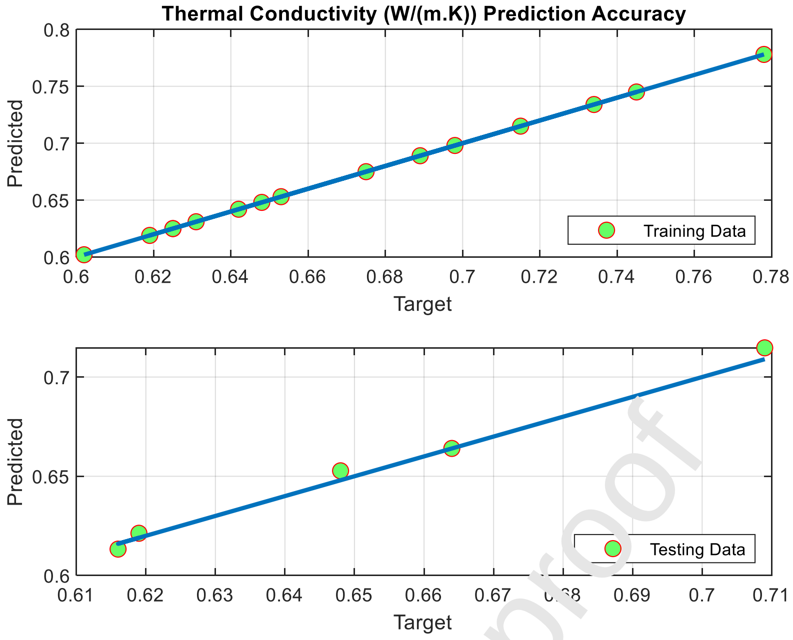

Fig. 12c. The thermal conductivity's fuzzy analysis prediction accuracy.

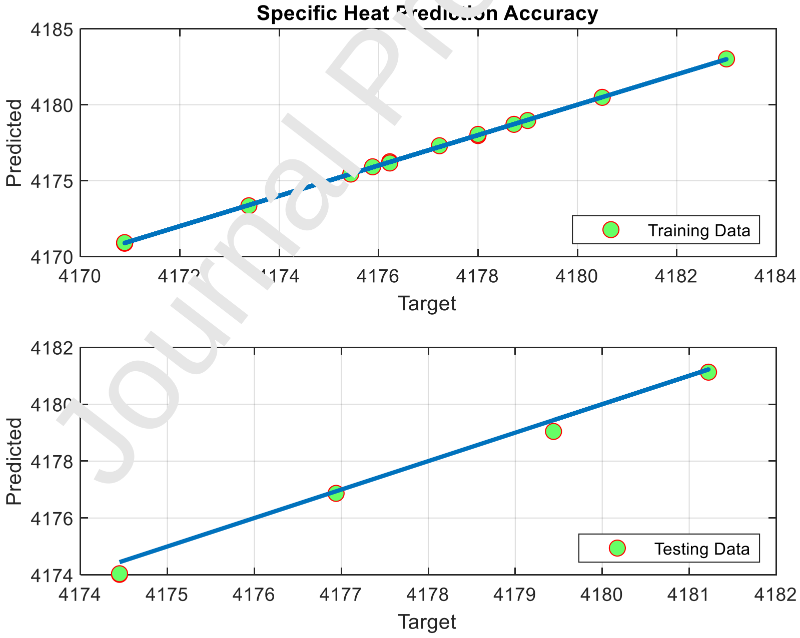

Fig.12d. The specific heat's fuzzy model prediction accuracy.

4.3.2 Determination of optimal parameters based on MPA

During the optimization phase and for a fair comparison, the values of the MPA parameters have been kept fixed for all optimization runs. In other words, the number of agents (particles or solutions) was kept at a value of 20, and the maximum number of iterations was kept at a value of 100. Furthermore, the upper and lower temperatures were 60 and 20, respectively, while the nanofluid material percentage was 0.2 and 0, respectively.

The optimization is done first to optimize each output as a single object. Thus, W and Y in Equation (3) become W = 1 and Y= y_n, respectively; where, n = 1, 2, 3, and 4, which refers to the output index. Then, multi-objective optimization takes place in two cases; first, to look for the optimal value withing the input-output search space, and second, to find out which experiment produces the optimal case. The MPA optimizer was applied in all the cases, and the results are illustrated in Table 3. The table compares the optimizer findings with the experimental data for single-objective cases. From the table, it can be noticed that density can have a much lower value than that obtained experimentally. However, a value of 973.743403 g/cm^3 can be the result when the temperature is lowered to 56.258382^{o}C with no nanofluid material.

On the other hand, the viscosity, thermal conductivity, and specific heat all match with the experimental data. In Case 1 of multi-objective optimization, the optimizer produced optimal values that occurred at a temperature of 60^{o}C and a percentage of 0.056005 of nanofluid material. According to the optimizer results of Case 2, the temperature at 60^{o}C and the nanofluid percentage at 0.05 are the optimal conditions that provide the best density, viscosity, thermal conductivity, and specific heat among all the experimental cases— it is worth mentioning that all swarm optimizations are based on random processes. Therefore, to avoid the doubt of obtaining the results randomly, the MPA optimizer was executed 100 times. The whole runs were found to produce the same results. Consequently, the optimizer's results are reliable and trustworthy.

Table 3: Proposed strategy optimal parameters compared to those obtained experimentally

Method	**Optimization Type**	**Controlling Variables**		**Controlled Variables**			
		Temperature (℃)	**Particles loading (wt.%)**	**Density**	**Viscosity**	**Thermal Conductivity**	**Specific Heat**
Experimental	Single	60	0	**985 (Min)**	**0.478 (Min)**	0.653	**4183 (Max)**
	Single	60	0.2	989.62	0.81658	**0.778 (Max)**	4175.88
Optimal using ANFIS & MPA	Single	56.26	0	**973.74**	0.53	0.65	4182.02
	Single	60	0	985.01	**0.48**	0.65	4183.02
	Single	60	0.2	989.62	0.80	**0.78**	4175.91
	Single	60	0	985.01	0.48	0.65	**4183.02**
Optimal using	Multi	60	0.056	986.28	0.57	0.72	4180.90

ANFIS & MPA (Case1)							
Optimal using ANFIS & MPA (Case2)	Multi	60	0.05	986.14	0.56	0.72	4181.13

The movements of the swarm agents that represent the proposed solutions during the optimization process were plotted against the iteration number to show the solutions' convergence. Figures (13a), (13b), and (13c) illustrate the solution agents' convergence curves throughout the optimization process for the objective function, temperature, and the nanofluid material percentage. The figures illustrate that the solutions converge after approximately 70 iterations, which indicates that the value of 100 as a maximum number of iterations is fair. Furthermore, the crowded plots of the solution agents (particles) at the beginning of the optimization process show that several solutions were proposed before the convergence occurred. Also, it is worth mentioning that the negative value of the cost function shown in Figure 13a indicates that the sum of the normalized outputs to be maximized is more significant than the sum of the normalized outputs to be minimized.

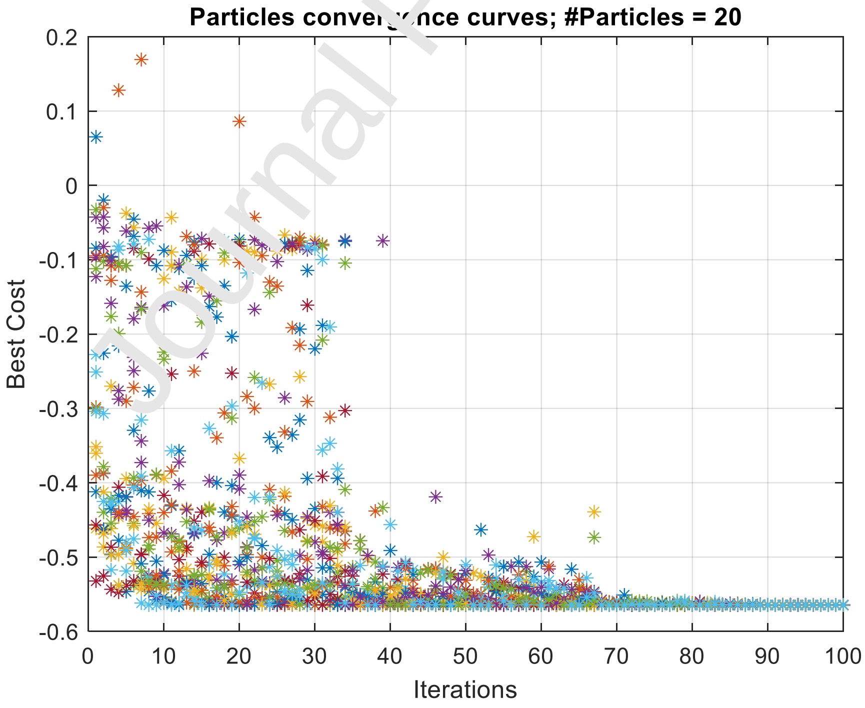

Fig. 13a. 1 Output's solution agents' convergence curve

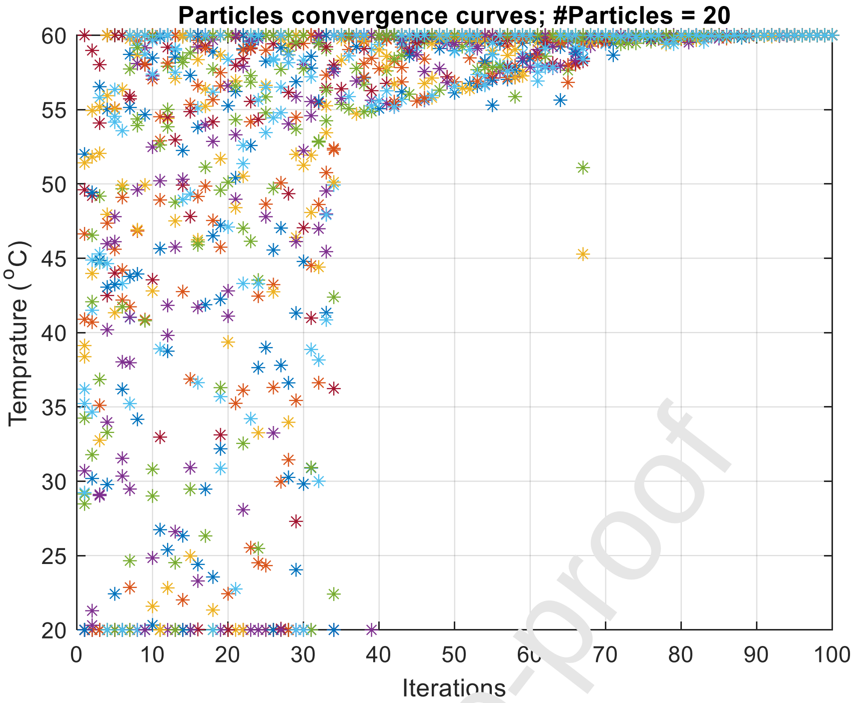

Fig. 13b. Temperature's solution agents' convergence curve

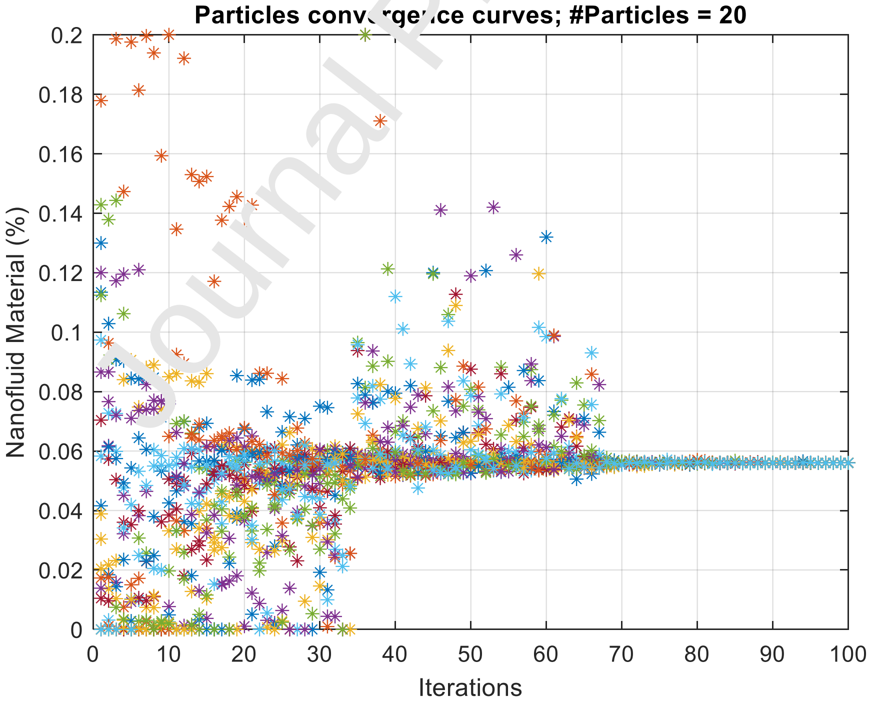

Fig. 13c. Nanofluid material percentage's solution agents' convergence curve

Until now, the optimization process had been performed within the experiment's upper and lower limits of the controlling variables. To maximize the benefits from the obtained fuzzy models, these limits were extended in both lower and upper directions by 5, 10, 15, 20, and 25 percent. This strategy was proposed to find out an optimal point outside the inputs' domain of the experimental data. Therefore, the optimization process was executed once again at each percent of the extended searching domain. The process was implemented for both single and multi-objective optimizations.

Table 4: The results for single and multi-objective optimization in the extended search domain

Objective function	**Extension (%)**	**Controlling Variables**		**Controlled Variables**			
		Temperature (^oC)	**Particles loading (wt.%)**	**Density**	**Viscosity**	**Thermal Conductivity**	**Specific Heat**
Density	5	56.258382	0	973.743403	0.532234	0.648818	4182.01987
	10	56.258386	0	973.743403	0.532234	0.648818	4182.019871
	15	56.258382	0	973.743403	0.532234	0.648818	4182.01987
	20	56.258382	0	973.743403	0.532234	0.648818	4182.01987
	25	56.258382	0	973.743403	0.532234	0.648818	4182.01987
Viscosity	5	63	0	1010.829728	0.428685	0.656518	4183.835442
	10	66	0	1048.667238	0.377977	0.660367	4184.654658
	15	69	0	1094.352174	0.326821	0.664904	4185.474615
	20	72	0	1144.507196	0.275530	0.670832	4186.294211
	25	75	0	1196.984383	0.224199	0.679495	4187.113183
Thermal Conductivity	5	63	0.21	1015.865518	0.769150	0.805964	4184.671268
	10	66	0.22	1053.888850	0.736247	0.840268	4193.431522
	15	69	0.23	1099.634213	0.701604	0.879148	4202.191398
	20	72	0.24	1149.797024	0.665319	0.920654	4210.951029
	25	75	0.25	1202.265861	0.628174	0.963390	4219.710541
Specific Heat	5	63	0.21	1015.865518	0.769150	0.805964	4184.671268
	10	66	0.22	1053.888850	0.736247	0.840268	4193.431522
	15	69	0.23	1099.634213	0.701604	0.879148	4202.191398
	20	72	0.24	1149.797024	0.665319	0.920654	4210.951029
	25	75	0.25	1202.265861	0.628174	0.963390	4219.710541
Multi-objective (Case 1)	5	63	0.059621	1012.246952	0.523923	0.738936	4181.575636
	10	66	0.069898	1050.432051	0.489651	0.772335	4182.008950
	15	69	0.102893	1097.159869	0.491226	0.843757	4181.436581

	20	72	0.096754	1147.241632	0.430124	0.886932	4182.615842
	25	75	0.086271	1199.432497	0.362041	0.928519	4183.882418

From Table 4, it can be noticed that in a single optimization of the density, the lowest value is only found at a temperature of 56.258382^{o} C with no nanofluid mixture, and there are no benefits of extending the search space. However, the viscosity decreases by increasing the temperature but with the absence of the nanofluid material. On the other hand, the thermal conductivity is proportional to both temperatures as well as the percentage of the nanofluid material. Similarly, the specific heat also increases with the increase of both controlling variables.

In the case of multi-objective optimization, the degree of improvement in each output is measured relative to the data of the optimal experiment (refer to Case 2 in Table 2). The percentages of gains are calculated according to Equation (6).

$$G_n = (-1)^M \frac{R-V}{R} * 100 \quad (6)$$

where, G_n is the gain of output *n*; *n* = [1, 2, 3, 4]; *R* is the value of the output obtained at the optimal experiment (reference value); *V* is the corresponding output found through the extended range; M takes a value of 0 or 1 in case of minimization and maximization, respectively.

An output with a positive gain indicates that there is an improvement in this output and vice versa. In a certain condition, the overall improvement ζ is calculated as the sum of the gains of the four outputs as in Equation (7).

$$\zeta = \sum_{n=1}^{4} G_n \quad (7)$$

Based on Equation (7), Table 5 shows the values of the gains and the improvement measure in each state of the extending range of the inputs.

Table 5: The improvement measure and the gains of the outputs resulting from the optimization with the extended range

Extension (%)	G_1	G_2	G_3	G_4	ζ
5	-2.64577	6.051428	4.222285	0.008457719	7.636396
10	-6.51789	12.197	8.933004	0.018821053	14.63093
15	-11.2563	11.91457	19.00663	0.005132016	19.67006
20	-16.3348	22.87123	25.09619	0.033335757	31.666
25	-21.6271	35.07971	30.96178	0.063627762	44.478

From Table 4 and based on the improvements measure presented in Table 5, it can be noticed that the total outputs except density show improvement by extending the search space. Also, the overall improvement measure I increases with the extended range. A vast improvement in the extended range is noticed on the viscosity and thermal conductivity, as shown from the values of G_2 and G_3, respectively. Therefore, the proposed methodology succeeded in finding out the optimal values of the current system, not only in the case of experimental search-space but also when the inputs' domain was extended within a specific range. Utilizing appropriate optimization algorithms, the relative error between the actual data and the prediction models can be reduced, which is highly significant for the precision of the models. Therefore, future studies must focus on comprehensive modelling that is applicable to different kinds of nanofluids.

Further research work can be carried out for higher particle volume fraction, particle shape, particle size and higher temperatures for predicting the thermophysical properties of models utilizing different assessment tools and modeling for the nanofluids investigated in this work. The prepared hybrid nanoparticles can also be suspended in different base fluids such as oil and molten salts for applications that requires high temperatures.

5. Conclusions

In this study, rGO/Co_3O_4 nanocomposite was synthesized, characterized, and then the thermophysical properties were obtained experimentally, after which the experimental data at varying values of temperature and particle loadings was used for optimization purposes. The study was concerned with different values of the controlling parameters. The *in-situ*/chemical reduction technique was used to synthesize the rGO/Co_3O_4 nanocomposite and then characterized with x-ray diffraction, transmission electron microscope, and magnetometry. The system was studied at temperature values of 20, 30, 40, 50, and 60℃ and with 0.05%, 0.1% and 0.2% volume concentrations. The rGO/Co_3O_4 nanocomposite nanofluid thermal conductivity and viscosity were investigated experimentally, and a maximum increment of 19.14% and 70.33% with 0.2% particle loadings at a temperature of 60^{o}C was obtained. At 0.05%, 0.1%, and 0.2% particle loading wt.%, the density increased by 0.115%, 0.23%, and 0.451% at a temperature of 20℃. Simultaneously, density increased by 0.117%%, 0.235%, and 0.469% respectively, at a temperature of 60℃, compared to water. At 0.2 wt.%, specific heat got reduced by 0.192% and 0.194% at 20^{o}C and 60^{o}C, respectively. When compared with water, no significant effect with the increase in temperature was observed: a similar trend as that of the water was followed by the prepared nanofluids. The main goal of this work is to determine the optimal values of temperature and the nanoparticle concentration that reduce the density and viscosity and maximize thermal conductivity and specific heat in a nanofluid mixture. An ANFIS model as an AI tool has been built for each output. Based on the four models, a recent MPA optimizer has been applied. The optimization process was implemented as a single and multi-objective optimization. The optimal values were found to be at 60℃ and a percentage of 0.056 of nanofluid material. However, among the conducted experiments, the optimizer pointed out that the optimal experiment is the one conducted at 60 ℃ and with a nanofluid percentage at 0.05. To benefit from the modelling technique, the optimization was executed outside the experimental input space by extending the searching domain by 5, 10, 15, 20, and 25%. This procedure was implemented for both single and multi-objective optimization. The results showed that there is an improvement when the inputs' range is extended. In conclusion, the proposed methodology of modelling with an AI tool such as ANFIS technique and then determining the optimal parameters with the MPA accomplished the goal of the work with huge success.

Appendix: Uncertainty analysis

Q_c = Conduction heat (W)
Q_S = Heat supplied (W)
V = Voltage
I = Current
k_{nf} = thermal conductivity of nanofluuids (W/mK)
d_m = mean diameter of the needle (m)
L = length of needle (m)
Δt = temperature difference (^{o}C)
R = resistance of the needle

(i) Thermal conductivity

(a) $$Q_c = \frac{k_{nf}\, \pi\, d_m L\, (\Delta t)}{(\Delta r)} \tag{A1}$$

(b) $$k_{nf} = \frac{Q_{Ele}(\Delta r)}{\pi d_m L(\Delta t)} \tag{A2}$$

(c) $$Q_s = \frac{V^2}{R} \tag{A3}$$

(d) $$\frac{U_{Q_S}}{Q_S} = \sqrt{\left(2\frac{U_V}{V}\right)^2 + \left(\frac{U_R}{R}\right)^2} \tag{A4}$$

By combining all the parameters, the uncertainty of thermal conductivity is

$$\frac{U_k}{k} = \sqrt{\left(2\frac{U_V}{V}\right)^2 + \left(\frac{U_R}{R}\right)^2 + \left(\frac{U_{T_1}}{T_1}\right)^2 + \left(\frac{U_{T_2}}{T_2}\right)^2 + \left(\frac{U_L}{L}\right)^2 + \left(\frac{U_{r_1}}{r_1}\right)^2 + \left(\frac{U_{r_2}}{r_2}\right)^2}$$

$$\frac{U_k}{K} = \sqrt{\left(2\frac{0.1}{220}\times 100\right)^2 + \left(\frac{0.1}{20}\times 100\right)^2 + \left(\frac{0.1}{60}\times 100\right)^2 + \left(\frac{0.1}{30}\times 100\right)^2 + (0.1)^2 + (0.1)^2 + (0.1)^2}$$

$$= 0.652\%$$

(ii) **Specific heat**:

(a) $Q_c = \dot{m}C_p(\Delta t)$ (A5)

Heat gained by the fluid (Q_c) is equal to electrical heat supplied (Q_S)

Then, $C_p = \frac{Q_S}{\dot{m}(\Delta t)}$ (A6)

$$Q_s = \frac{V^2}{R}$$

$$\frac{U_{Q_S}}{Q_S} = \sqrt{\left(2\frac{U_V}{V}\right)^2 + \left(\frac{U_R}{R}\right)^2} \quad \text{(A7)}$$

By combining all the parameters, the uncertainty of specific heat is

$$\frac{U_{C_p}}{C_p} = \sqrt{\left(2\frac{U_V}{V}\right)^2 + \left(\frac{U_R}{R}\right)^2 + \left(\frac{U_{\dot{m}}}{\dot{m}}\right)^2 + \left(\frac{U_{T_1}}{T_1}\right)^2 + \left(\frac{U_{T_2}}{T_2}\right)^2}$$

$$= \sqrt{\left(2\frac{0.1}{220}\times 100\right)^2 + \left(\frac{0.1}{20}\times 100\right)^2 + \left(\frac{0.1}{60}\times 100\right)^2 + \left(\frac{0.1}{60}\times 100\right)^2 + \left(\frac{0.1}{30}\times 100\right)^2}$$

$$= 0.6505\%$$

Acknowledgement

The authors would like to thank Ms. Shabnam Fatima, English language instructor, at English Language Centre at University of Sharjah for her assistance with the English proof reading.

References

[1] N.K. Cakmak, Z. Said, L.S. Sundar, Z.M. Ali, A.K. Tiwari, Powder Technology (2020).
[2] S.U. Choi, J.A. Eastman, Argonne National Lab., IL (United States), 1995.
[3] A.A. Hachicha, B.A. Yousef, Z. Said, I. Rodríguez, Renewable and Sustainable Energy Reviews 112 (2019) 280.
[4] C. Nguyen, F. Desgranges, N. Galanis, G. Roy, T. Maré, S. Boucher, H.A. Mintsa, International Journal of Thermal Sciences 47 (2008) 103.
[5] M.H. Esfe, S. Saedodin, O. Mahian, S. Wongwises, Journal of Thermal Analysis and Calorimetry 117 (2014) 675.
[6] L.S. Sundar, Y.T. Sintie, Z. Said, M.K. Singh, V. Punnaiah, A.C. Sousa, Sustainable Energy Technologies and Assessments 40 (2020) 100772.
[7] A.A. Arani, J. Amani, Experimental Thermal and Fluid Science 42 (2012) 107.
[8] M. Gupta, V. Singh, Z. Said, Sustainable Energy Technologies and Assessments 39 (2020) 100720.
[9] Z. Said, M.E.H. Assad, A.A. Hachicha, E. Bellos, M.A. Abdelkareem, D.Z. Alazaizeh, B.A. Yousef, Renewable and Sustainable Energy Reviews 112 (2019) 183.
[10] H.E. Patel, T. Sundararajan, S.K. Das, Journal of Nanoparticle Research 12 (2010) 1015.
[11] Y.-j. Hwang, J. Lee, C. Lee, Y. Jung, S. Cheong, C. Lee, B. Ku, S. Jang, Thermochimica Acta 455 (2007) 70.
[12] Z. Said, A. Allagui, M.A. Abdelkareem, H. Alawadhi, K. Elsaid, Journal of colloid and interface science 520 (2018) 50.
[13] M. Sheikholeslami, M. Jafaryar, Z. Said, A.I. Alsabery, H. Babazadeh, A. Shafee, Applied Thermal Engineering (2020) 115935.
[14] Z. Said, S. Arora, E. Bellos, Renewable and Sustainable Energy Reviews 94 (2018) 302.

[15] E. Bellos, Z. Said, C. Tzivanidis, Journal of cleaner production 196 (2018) 84.
[16] Z. Said, M.A. Abdelkareem, H. Rezk, A.M. Nassef, Powder Technology 353 (2019) 345.
[17] Z. Said, R. Saidur, Nanofluid heat and mass transfer in engineering problems (2017) 39.
[18] Z. Said, R. Saidur, M. Sabiha, A. Hepbasli, N. Rahim, Journal of cleaner production 112 (2016) 3915.
[19] Z. Said, M.H. Sajid, M.A. Alim, R. Saidur, N.A. Rahim, International communications in heat and mass transfer 48 (2013) 99.
[20] Z. Said, International Communications in Heat and Mass Transfer 78 (2016) 207.
[21] Z. Said, R. Saidur, A. Hepbasli, N. Rahim, International communications in heat and mass transfer 58 (2014) 85.
[22] Z. Said, A. Kamyar, R. Saidur, IOP conference series: earth and environmental science, IOP Publishing, 2013, p. 012002.
[23] Z. Said, S. Rahman, M.E.H. Assad, A.H. Alami, Sustainable Energy Technologies and Assessments 31 (2019) 306.
[24] A.A. Hachicha, Z. Said, S. Rahman, E. Al-Sarairah, Renewable Energy (2020).
[25] Z. Said, R. Saidur, M. Sabiha, N. Rahim, M. Anisur, Solar Energy 115 (2015) 757.
[26] Z. Said, R. Saidur, N.A. Rahim, M.A. Alim, Energy and Buildings 78 (2014) 1.
[27] S. Pei, H.-M. Cheng, Carbon 50 (2012) 3210.
[28] U. Tanaka, T. Sogabe, H. Sakagoshi, M. Ito, T. Tojo, Carbon 39 (2001) 931.
[29] F. Ortmann, W.G. Schmidt, F. Bechstedt, Physical review letters 95 (2005) 186101.
[30] Z. Said, M.A. Abdelkareem, H. Rezk, A.M. Nassef, H.Z. Atwany, Powder Technology 364 (2020) 795.
[31] L. Sundar, E. Venkata Ramana, Z. Said, A. Pereira, A. Sousa, Journal of Thermal Science and Engineering Applications (2020) 1.
[32] Q. Su, W. Yuan, L. Yao, Y. Wu, J. Zhang, G. Du, Materials Research Bulletin 72 (2015) 43.
[33] P. Shi, X. Dai, H. Zheng, D. Li, W. Yao, C. Hu, Chemical Engineering Journal 240 (2014) 264.
[34] C. Xiang, M. Li, M. Zhi, A. Manivannan, N. Wu, Journal of Power Sources 226 (2013) 65.
[35] L.S. Sundar, M.K. Singh, M. Ferro, A.C. Sousa, International Communications in Heat and Mass Transfer 84 (2017) 1.
[36] M.U. Sajid, H.M. Ali, International Journal of Heat and Mass Transfer 126 (2018) 211.
[37] D. Toghraie, V.A. Chaharsoghi, M. Afrand, Journal of Thermal Analysis and Calorimetry 125 (2016) 527.
[38] S.S. Harandi, A. Karimipour, M. Afrand, M. Akbari, A. D'Orazio, International Communications in Heat and Mass Transfer 76 (2016) 171.
[39] M. Afrand, Applied Thermal Engineering 110 (2017) 1111.
[40] M.J. Nine, M. Batmunkh, J.-H. Kim, H.-S. Chung, H.-M. Jeong, Journal of nanoscience and nanotechnology 12 (2012) 4553.
[41] N.N. Esfahani, D. Toghraie, M. Afrand, Powder Technology 323 (2018) 367.
[42] O. Soltani, M. Akbari, Physica E: Low-dimensional Systems and Nanostructures 84 (2016) 564.
[43] A. Alirezaie, S. Saedodin, M.H. Esfe, S.H. Rostamian, Journal of Molecular Liquids 241 (2017) 173.
[44] A. Zareie, M. Akbari, Journal of Molecular Liquids 230 (2017) 408.
[45] L.S. Sundar, M.K. Singh, A.C. Sousa, International Communications in Heat and Mass Transfer 52 (2014) 73.
[46] G. Huminic, A. Huminic, International Journal of Heat and Mass Transfer 125 (2018) 82.
[47] M. Gupta, V. Singh, S. Kumar, S. Kumar, N. Dilbaghi, Z. Said, Journal of cleaner production 190 (2018) 169.
[48] R.R. Sahoo, V. Kumar, International Communications in Heat and Mass Transfer 111 (2020) 104451.
[49] P. Kishore, V. Sireesha, V.S. Harsha, V.D. Rao, A.B. Solomon, Materials Today: Proceedings (2020).
[50] Z. Said, M. Gupta, H. Hegab, N. Arora, A.M. Khan, M. Jamil, E. Bellos, The International Journal of

Advanced Manufacturing Technology 105 (2019) 2057.
[51] W.S. Hummers Jr, R.E. Offeman, Journal of the american chemical society 80 (1958) 1339.
[52] M. Ghasemi, A.M. Nassef, M. Al-Dhaifallah, H. Rezk, International Journal of Energy Research (2020).
[53] A. Faramarzi, M. Heidarinejad, S. Mirjalili, A.H. Gandomi, Expert Systems with Applications (2020) 113377.
[54] H. Yang, Y. Su, C. Shen, T. Yang, H. Gao, Surface and Interface Analysis: An International Journal devoted to the development and application of techniques for the analysis of surfaces, interfaces and thin films 36 (2004) 155.
[55] L.S. Sundar, E.V. Ramana, M. Singh, A. De Sousa, Chemical physics letters 554 (2012) 236.
[56] F. Mohandes, F. Davar, M. Salavati-Niasari, Journal of magnetism and magnetic materials 322 (2010) 872.
[57] P. Dutta, M. Seehra, S. Thota, J. Kumar, Journal of Physics: Condensed Matter 20 (2007) 015218.
[58] M. Chandrasekar, S. Suresh, A.C. Bose, Experimental Thermal and Fluid Science 34 (2010) 210.
[59] J. Avsec, M. Oblak, International Journal of Heat and Mass Transfer 50 (2007) 4331.
[60] T.R. Shah, H. Koten, H.M. Ali, Hybrid Nanofluids for Convection Heat Transfer, Elsevier, 2020, p. 179-213.
[61] P.K. Namburu, D.P. Kulkarni, D. Misra, D.K. Das, Experimental Thermal and Fluid Science 32 (2007) 397.
[62] L. Fedele, L. Colla, S. Bobbo, International journal of refrigeration 35 (2012) 1359.
[63] H.D. Koca, S. Doganay, A. Turgut, I.H. Tavman, R. Saidur, I.M. Mahbubul, Renewable and Sustainable Energy Reviews 82 (2018) 1664.
[64] H. Yarmand, S. Gharehkhani, S.F.S. Shirazi, M. Goodarzi, A. Amiri, W.S. Sarsam, M.S. Alehashem, M. Dahari, S. Kazi, International Communications in Heat and Mass Transfer 77 (2016) 15.

Declaration of competing interests

☒ The authors declare that they have no known competing financial interests or personal relationships that could have appeared to influence the work reported in this paper.

☐The authors declare the following financial interests/personal relationships which may be considered as potential competing interests:

CRediT author statement

Zafar Said: Supervision, Conceptualization, Methodology, Visualization, Data curation, Writing- Original draft preparation, Writing- Reviewing and Editing, Graphical Abstract, Highlights.

L. Syam Sundar: Visualization, Conceptualization, Methodology, Data curation, Writing- Original draft preparation, Writing- Reviewing and Editing.

Hegazy Rezk: Conceptualization, Methodology, Data curation, Writing- Original draft preparation, Writing- Reviewing and Editing.

Ahmed M. Nassef : Conceptualization, Methodology, Data curation, Writing- Original draft preparation, Writing- Reviewing and Editing.

Hafiz Muhammad Ali: Writing- Original draft preparation, Writing- Reviewing and Editing.

Mohsen Sheikholeslami: Writing- Original draft preparation, Writing- Reviewing and Editing.

Graphical Abstract:

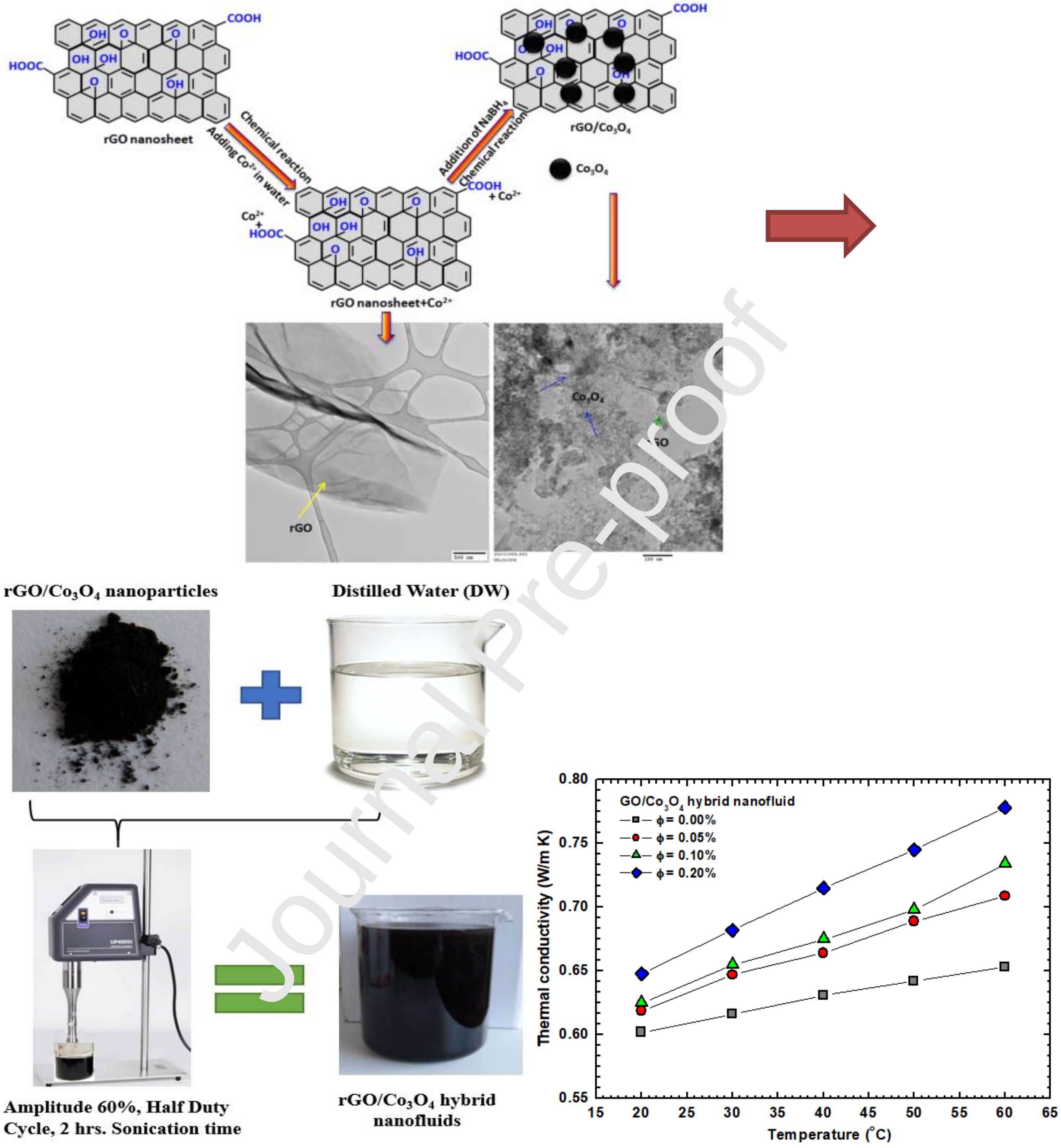

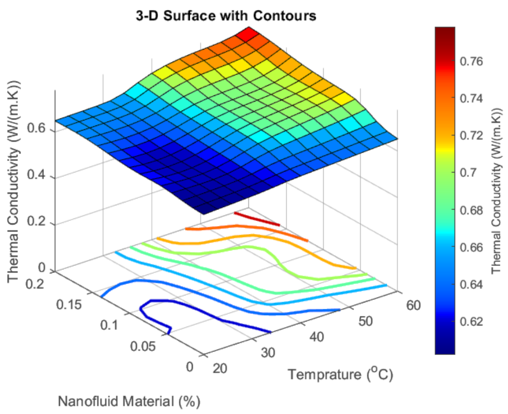
3-D Surface with Contours
Thermal Conductivity (W/(m.K))
0.6
0.4
0.2
0
0.2
0.15
0.1
0.05
0
20
30
40
50
60
Temprature (°C)
Nanofluid Material (%)
0.76
0.74
0.72
0.7
0.68
0.66
0.64
0.62
Thermal Conductivity (W/(m.K))

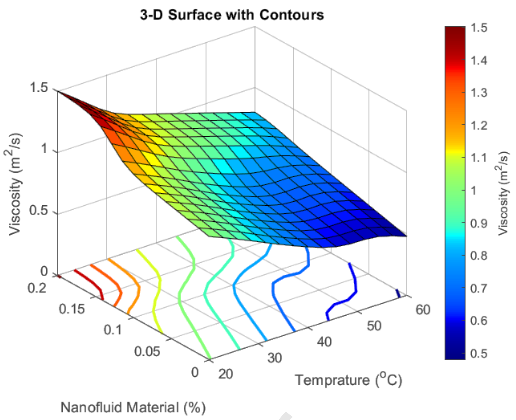
3-D Surface with Contours
Viscosity (m^2/s)
1.5
1
0.5
0
0.2
0.15
0.1
0.05
0
20
30
40
50
60
Temprature (°C)
Nanofluid Material (%)
1.5
1.4
1.3
1.2
1.1
1
0.9
0.8
0.7
0.6
0.5
Viscosity (m^2/s)

Highlights

- Novel rGO/Co_3O_4 nanocomposite is synthesized and characterized.
- Increment of 19.14% with 0.2% particle loadings at 60°C was obtained for thermal conductivity.
- Increment of 70.83% with 0.2% particle loadings at 60°C was obtained for viscosity.
- A maximum reduction in specific heat is 0.194% at 60℃.
- Optimal values were found to be at 60 ℃ and 0.056 % of particle loading.